Syndecan-4 controls lymphatic vasculature remodeling during embryonic development

DOI:
10.1242/dev.140129

Document Version
Accepted author manuscript

Development Advance Online Articles. First posted online on 27 October 2016 as 10.1242/dev.140129
Access the most recent version at http://dev.biologists.org/lookup/doi/10.1242/dev.140129

Syndecan-4 controls lymphatic vasculature remodeling during embryonic development

Yingdi Wang[1], Nicolas Baeyens[1,*], Federico Corti[1], Keiichiro Tanaka[1], Jennifer S. Fang[1], Jiasheng Zhang[1], Yu Jin[1], Brian Coon[1], Karen K. Hirschi[1, 4], Martin A. Schwartz[1, 2, 3], Michael Simons[1, 2,‡]

[1]Yale Cardiovascular Research Center, Department of Internal Medicine; [2]Department of Cell Biology; [3]Department of Biomedical Engineering; [4]Yale Stem Cell Center, Yale University School of Medicine, New Haven, CT 06511, USA

[*]Present address: Wellcome Trust Centre for Cell-Matrix Research, Faculty of Life Sciences, Manchester, United Kingdom

‡ Author for correspondence (michael.simons@yale.edu)

KEY WORDS: syndecan-4, lymphatic remodeling, embryonic development

ABSTRACT

The role of fluid shear stress in vasculature development and remodeling is well appreciated. However, the mechanisms regulating these effects remain elusive. We show that abnormal flow sensing in lymphatic endothelial cells (LECs) caused by *Sdc4* or *Pecam-1* deletion in mice results in impaired lymphatic vessel remodeling including abnormal valve morphogenesis. Ablation of either gene leads to formation of irregular, enlarged, and excessively branched lymphatic vessels. In both cases, lymphatic-valve-forming endothelial cells are randomly oriented, resulting in formation of abnormal valves. These abnormalities are much more pronounced in *Sdc4*$^{-/-}$;*Pecam-1*$^{-/-}$ double knockout mice that develop severe edema. *In vitro*, *SDC4*-knockdown LECs fail to align under flow and exhibit high expression of the planar cell polarity protein VANGL2. Reducing VANGL2 levels in *SDC4*-knockdown LECs restores their alignment under flow while its overexpression in wildtype LECs mimics flow-alignment abnormalities seen in *SDC4*-knockdown LECs. Syndecan-4 thus controls flow-induced LEC polarization via regulation of VANGL2 expression.

INTRODUCTION

Tissue remodeling is an important process during organogenesis. In the vascular system, fluid flow plays a critical role in the morphogenesis of both blood and lymphatic vasculature in a manner that is still poorly understood. Lymphatic vessels constitute a distinct vascular network which takes up interstitial fluid (lymph) and returns it to systemic circulation. The effective unidirectional transport of the lymphatic fluid requires formation of lymphatic intraluminal valves (hereafter referred to as lymphatic valves) that prevent backflow of lymph. A previous study has established that initiation of lymphatic fluid flow is required for the development of lymphatic valves, a process that involves transcription factors Prox1 and FoxC2 (Sabine et al., 2012). Flow is also required for the lymphatic fate maintenance (Chen et al., 2012), collecting lymphatic vessel maturation (Sweet et al., 2015) and lymphatic vessel stabilization (Sabine et al., 2015). Despite these data pointing to the role of fluid flow in lymphatic vasculature development, the molecular mechanisms involved in mechanotransduction in the lymphatic endothelium have not been established.

In the blood endothelial cells, fluid shear stress (FSS) signaling is mediated, in part, by a junctional mechanosensory complex that includes platelet and endothelial cell adhesion molecule-1 (PECAM-1), vascular endothelial cell cadherin (VE-cadherin) and vascular endothelial growth factor receptor 2 (VEGFR2) (Tzima et al., 2005). Recently, VEGFR3 has been identified as a new component of this mechanosensory complex (Coon et al., 2015). Interestingly, the levels of VEGFR3 expression regulate the sensitivity of endothelial cells (ECs) to FSS with higher expression leading to greater sensitivity to flow signal (Baeyens et al., 2015).

In addition to the mechanosensory complex described above, syndecan-4 has emerged as another regulator of FSS-induced ECs alignment (Baeyens et al., 2014). In addition to flow, syndecan-4 also has the ability to respond to directly applied mechanical tension (Bellin et

al., 2009). However, the molecular mechanism underlying syndecan-4-dependent shear stress response is unknown. Syndecan-4 is a transmembrane heparin sulfate proteoglycan that contributes to a number of cellular signaling events (Elfenbein and Simons, 2013). It has been implicated in regulation of fibroblast growth factor signaling (Elfenbein et al., 2012; Horowitz et al., 2002) in the endothelium, mechanical stress-induced activation of the calcineurin-NFAT pathway in cardiomyocytes (Finsen et al., 2011), and modulation of the Wnt/β-catenin pathway in *Xenopus* via interaction with LRP6 receptor (Astudillo et al., 2014). It also regulates Wnt/planar cell polarity (PCP) pathway during convergent extension (Muñoz et al., 2006), and induces clathrin-mediated endocytosis in PCP signaling (Ohkawara et al., 2011). In mouse, syndecan-4 has been shown to interact genetically with the core PCP protein Vang-like 2 (Vangl2), through which it regulates neural tube closure, wound healing and stereocilia orientation in the sensory hair cells (Escobedo et al., 2013).

Given this involvement of syndecan-4 and PECAM-1 in mechanotransduction, we set out to study the role of these proteins in lymphatic vasculature development. We find that deletion of either *Sdc4* or *Pecam-1* in mice resulted in abnormal lymphatic vessel remodeling and, in particular, abnormal lymphatic valve formation due to the failure of lymphatic-valve-forming ECs to properly align under flow. A deletion of both genes resulted in more profound abnormalities than that of individual genes. Finally, in the case of *Sdc4* deletion, these effects were mediated by an abnormal flow-induced increase in Vangl2 levels.

RESULTS

Lymphatic vessels show remodeling defect in *Sdc4*$^{-/-}$ mice

To study the function of syndecan-4 in lymphatic vasculature formation, we used the development of mesenteric vessels as a model. In control mice, small diameter, cord-like lymphatic endothelial structures (Prox1+, Vegfr3+, VE-cadherin+) are present by embryonic stage (E)14.5 (Fig. S1A, white arrow). The LECs in these vessels extend fine cellular

processes to connect to each other (Fig. S1A, yellow arrow). By E15.5, larger diameter lymphatic tubular structures are formed (Fig. S1A, arrow) and a complex, honeycombed primary lymphatic plexus (Prox1+, Vegfr3+) is developed by E16.5 (Fig. S1B). This primary lymphatic plexus is then remodeled into a complete lymphatic vascular network including capillaries (Fig. 1A, yellow arrow) and collecting lymphatic vessels (Fig. 1A,B, white arrows).

In *Sdc4*$^{-/-}$ mice, the development of mesenteric lymphatic vessels is similar to control from E14.5 through E16.5 (Fig. S1A,B). However, abnormal lymphatic vessels are observed in the mutants at later embryonic stages (Fig. 1C,D, arrows). At E18.5, instead of forming a hierarchal vascular network (Fig. 1A,B, arrows), mesenteric lymphatic vessels in *Sdc4* knockouts tend to form a vascular plexus with multiple branches (Fig. 1C, arrows). Compared with littermate controls, cell-cell junctions in *Sdc4*$^{-/-}$ mice are less linear and show numerous protrusions exhibiting a wavy appearance (Fig. S1C). Moreover, enlarged, irregular lymphatic vessels are frequently seen in *Sdc4* nulls (Fig. 1D, arrows). To determine the cause of increased lymphatic vessel diameter in *Sdc4*$^{-/-}$, we examined cell cycle distribution of LECs and BECs in the mutants using Flow-Assisted Cell Sorting (FACS) (Fig. S2A,B). The number of LECs in S/G2/M phases of the cell cycle was increased in *Sdc4*$^{-/-}$ mice compared with controls (Fig. S2A) suggesting increased proliferation. Importantly, this was not seen in BECs in *Sdc4* knockouts (Fig. S2B). This data is consistent with increased lymphatic but not blood vessel diameter in *Sdc4*$^{-/-}$ mice.

Prox1^{high} lymphatic-valve-forming ECs in *Sdc4* nulls are abnormally oriented

Given these remodeling abnormalities, we set out to investigate the development of lymphatic valves, an important event during lymphatic vasculature remodeling. In control mice, lymphatic valves start to develop in mesenteric lymphatic vessels at E16.5 (Sabine et al., 2012; Tatin et al., 2013). This is also the time when flow begins (Sabine et al., 2012). In

agreement with previous reports (Sabine et al., 2012; Tatin et al., 2013), the development of lymphatic valves in control mice begins by the formation of clusters of Prox1^{high} lymphatic-valve-forming ECs that are initially aligned along the longitudinal axis of lymphatic vessels (Fig. S1D, arrow). Valve-forming cells subsequently reorient 90° and become perpendicular to flow direction (Fig. 1E, left). During this reorientation process, the nuclei of Prox1^{high} valve-forming cells show morphological and organization changes becoming highly elongated (Fig. 1E, left, arrowheads), and are tightly packed (Fig. 1E, left). Furthermore, nuclear morphology and orientation are highly correlated with cell morphology and cell orientation (Fig. S3). In contrast, in *Sdc4*$^{-/-}$ mice, the nuclei of Prox1^{high} cells are rounded (Fig. 1F, left, arrowheads), randomly oriented (Fig. 1F, left), and loosely organized (Fig. 1F, left).

Since it is more accurate to measure nuclear orientation than cell orientation, we assessed valve-forming cell orientation by measuring the angle of nuclei relative to flow direction (Fig. 1G). In control mice, the majority of valve-forming cells (87 %) are oriented ≥ 45 ° relative to flow direction at E17.5 (Fig. 1G). In *Sdc4* nulls, even though the formation of lymphatic valves begins normally (Fig. S1D, arrow), only 57 % of the valve-forming cells are oriented ≥ 45 ° (Fig. 1G). Nearly half of the valve-forming cells (43 %) in *Sdc4* nulls are arranged within 45 ° relative to flow direction (Fig. 1G).

The morphology of Prox1^{high} LECs was examined by measuring the roundness of the nuclei (Fig. 1H). In agreement with immunostaining results (Fig. 1E, left, arrowheads and Fig. 1F, left, arrowheads), Prox1^{high} valve-forming cells in *Sdc4* nulls are less elongated than in controls (Fig. 1H). Moreover, Prox1^{high} valve-forming cells in *Sdc4*$^{-/-}$ are loosely organized and form wide band of cells (Fig. 1F, left, middle) while they are tightly packed in control embryos (Fig. 1E, left, middle). At E18.5, valve-forming cells in control animals reorient again to form mature lymphatic valves that have two leaflets (Fig. 1E, middle, arrowheads)

whereas in *Sdc4* knockouts, Prox1^{high} LECs exhibit similar organization as at E17.5 (Fig. 1F, middle). Also, some of the Prox1^{high} cells in *Sdc4* null do not reorient and remain parallel to the flow direction along lymphatic vessel wall (Fig. 1F, right, arrow). In contrast, Prox1^{high} LECs in control mice are concentrated in valve-forming areas (Fig. 1E, right, arrows).

We further investigated cell alignment by examining actin filament remodeling and alignment in lymphatic vessels. Phalloidin labeling showed that in control lymphatics, actin filaments are remodeled into long, fine fibers, which are aligned in the direction of flow (Fig. 2A). In contrast, in *Sdc4*$^{-/-}$, actin fibers of LECs have a short, thick appearance and are randomly organized (Fig. 2B).

To examine whether the abnormal reorientation of lymphatic-valve-forming cells in *Sdc4*$^{-/-}$ mice compromises lymphatic valve development, we quantified the formation of valves. In control E18.5 animals, the majority of lymphatic valves (88.5 %) are mature V-shape valves (Fig. 2C, arrows) although there are a small percentage of immature valves (11.5 %) with a ring-shape morphology (Fig. 2F). In contrast, in *Sdc4* nulls, mature lymphatic valves are rarely seen (9.3 %) at E18.5 (Fig. 2F). The majority of lymphatic valves in the mutants retaining the ring-shape appearance of immature valves (26 %) (Fig. 2D,F) or appearing highly abnormal (64.7 %) with Prox1^{high} valve-forming cells either randomly oriented or aligned parallel to flow direction (Fig. 2E,F).

Together, these data show that syndecan-4 is important in regulating Prox1^{high} lymphatic-valve-forming EC reorientation and lymphatic valve formation during embryonic development. While *Sdc4* null mice can survive till adulthood, abnormal lymphatic valves were also observed in dermal lymphatic vessels in *Sdc4*$^{-/-}$ adults (Fig. S4C,D, arrows).

Abnormal lymphatic vessel development in *Pecam-1* null mice

To establish whether abnormalities in lymphatic development noted in *Sdc4*$^{-/-}$ mice were due to abnormal shear stress sensing or perhaps other features of syndecan-4 biology, we examined lymphatic vessel morphogenesis in *Pecam-1* null mice that have a flow-sensing defect. As in *Sdc4*$^{-/-}$, *Pecam-1*$^{-/-}$ mice did not display any lymphatic abnormalities during early stages of embryonic development (E14.5 to E16.5, Fig. S5A-D, arrows and Fig. S5E,F). However, by E18.5, unlike littermate controls (Fig. 3A), these mutants develop irregular (Fig. 3B, arrow and Fig. S6B, arrows), enlarged (Fig. 3C, arrow, Fig. S6C, yellow arrows and Fig. S6G,H, arrows), and abnormally branched (Fig. 3D, arrow, Fig. S6C, white arrows and Fig. S6D, arrow) mesenteric lymphatic vessels.

FACS analysis of LECs and BECs isolated from mesenteries of E18.5 embryos demonstrated a decrease in the number of cells in S/G2/M phases of the cell cycle in *Pecam-1*$^{-/-}$ mice and increased number of the cells at G1 phase (Fig. S2C,D). Thus, increased cell proliferation does not account for increased vessel diameter seen in these animals.

Prox1^{high} valve-forming cells in *Pecam-1* nulls were less elongated (Fig. 3F, left, middle, arrowheads, Fig. 3G and Fig. S6I, arrow), randomly oriented (Fig. 3F, left, middle and Fig. S6I) and loosely organized (Fig. 3F, left, middle and Fig. S6I) compared to controls (Fig. 3E, left, middle, arrowheads and Fig. 3G). Moreover, some of the valve- forming cells in *Pecam-1*$^{-/-}$ fail to reorient and are aligned along lymphatic vessel wall (Fig. S6J, arrow). Prox1^{high} LECs that are not concentrated in valve-forming areas are often seen in *Pecam-1* nulls (Fig. 3F, right, arrow).

Unlike in control mice where the majority of Prox1^{high} valve-forming cells are oriented perpendicular to the flow direction at E17.5 (Fig. 3E, left, right, arrows) with the majority (85 %) of nuclei aligning at a $\geq$ 45 ° relative to the flow direction (Fig. 3H), in *Pecam-1*$^{-/-}$ mice, a

much smaller number of valve-forming cells (52 %) exhibited this degree of nuclear orientation (Fig. 3H). In agreement with these findings, actin filaments of LECs were not aligned with flow in *Pecam1*$^{-/-}$ mice (Fig. 4A,B).

The abnormal reorientation of valve-forming cells in *Pecam-1* nulls results in significantly reduced formation of mature lymphatic valves and the development of immature and abnormal valves at E18.5 (Fig. 4C-E and Fig. S6K-N, arrows).

Sdc4$^{-/-}$; _Pecam-1_$^{-/-}$ double knockout mice develop a severe lymphatic phenotype

To test a genetic interaction between syndecan-4 and Pecam-1 with regard to lymphatic vasculature development, we generated *Sdc4*$^{-/-}$; *Pecam1*$^{-/-}$ double knockout mice. Examination of the mesenteric lymphatic vessels revealed much more extensive abnormalities including irregular morphology (Fig. 5A, middle, white arrow), increased diameter (Fig. 5A, middle, yellow arrow) and abnormal branching (Fig. 5A, bottom, arrows) in *Sdc4*$^{-/-}$; *Pecam1*$^{-/-}$ animals than in mice with a single gene deletion. Blood-filled jugular lymph sac was observed in *Sdc4*$^{-/-}$; *Pecam1*$^{-/-}$ at E15.5 (Fig. S7). At E15.5, 8% of the *Sdc4*$^{-/-}$; *Pecam1*$^{-/-}$ embryos were lethal, 77% exhibited blood-filled lymphatic structures and/or edema, while 15% appeared normal. The *Sdc4*$^{-/-}$; *Pecam-1*$^{-/-}$ mice that lived till adulthood appeared normal and fertile.

Mural cell coverage in lymphatic vessels was somewhat increased in both *Sdc4*$^{-/-}$ and *Pecam-1*$^{-/-}$ embryos compared with controls (Fig. S8, arrows). However, the increase was much more extensive in *Sdc4*$^{-/-}$; *Pecam1*$^{-/-}$ double knockouts (Fig. 5B,C). Moreover, *Sdc4*$^{-/-}$; *Pecam-1*$^{-/-}$ mice developed abnormal lymphatic valves (Fig. 5E, arrows and Fig. 5F).

To investigate whether there is any compensation between syndecan-4 and Pecam-1, we examined Pecam-1 levels in lymphatic vessels in *Sdc4*$^{-/-}$ mice or syndecan-4 levels in *Pecam-1* nulls by qRT-PCR. No significant changes in expression were observed (Fig. S9A,B).

Vangl2 is up-regulated in *Sdc4*$^{-/-}$ mice

The reorientation defect of Prox^{high} valve-forming ECs observed in *Sdc4*$^{-/-}$ or *Pecam-1*$^{-/-}$ mutants is reminiscent of mice deficient in planar cell polarity (PCP) protein Vangl2 (Tatin et al., 2013). We therefore measured its expression in *SDC4* knockdown (KD) or *PECAM-1* KD LECs. Exposure to laminar flow increased Vangl2 levels in controls as well as in *SDC4* KD and *PECAM-1* KD LECs (Fig. 6A). However, the increase was much higher in *SDC4* KD LECs compared with controls (7 fold vs. 3 fold) while the increase was less in *PECAM-1* KD cells (Fig. 6A).

Similar results were observed *in vivo*. We isolated thoracic duct (TD) from wildtype (WT) and *Sdc4*$^{-/-}$ mice, respectively, and examined the expression levels of Vangl2 by qRT-PCR. Since TD contains a mixed pool of cell types, we normalized our qPCR results to Cdh5 (Fig. 6B). There was a significant (5.8 fold) increase in Vangl2 expression in *Sdc4*$^{-/-}$ compared to WT mice (Fig. 6B). In addition, there was a less profound (2.6 fold) increase of the PCP protein Celsr1 in *Sdc4* nulls (Fig. 6B) while Celsr1 levels in *Pecam-1*$^{-/-}$ mice appeared similar as in WT (Fig. S9C). To examine whether increased Vangl2 levels in *Sdc4* nulls mediate increased Celsr1 expression, we overexpressed VANGL2 in LECs (Fig. S9D) and tested CELSR1 expression in these cells using qRT-PCR. VANGL2 overexpression resulted in an increase in CELSR1 levels (Fig. S9E) that was similar to the *in vivo* results described above.

Syndecan-4 controls LEC response to flow signals through VANGL2

We postulated that an increase in Vangl2 levels was responsible for the mis-sensing of flow signals in *Sdc4* null LECs, leading to lymphatic vessel remodeling defects. To test this hypothesis, we first examined whether increased VANGL2 expression in LECs causes abnormal cell alignment to flow. To this end, LECs were transduced with a lentivirus

expressing VANGL2 (pLenti-VANGL2) or control virus and cell alignment was evaluated after exposure to flow. Since the flow is largely laminar in lymphatic vessels before mature, functional valves are developed, we subjected LECs to laminar flow in vitro. In the absence of flow (static condition), LECs are randomly oriented and thus display an average orientation of ~45 ° relative to flow direction (perfect alignment of all cells in flow direction is 0 °, and perpendicular alignment is 90 °). While LECs transduced with a control virus aligned normally to flow direction with an average orientation of ~33 °, VANGL2 overexpression almost fully inhibited cells' ability to align to flow with an average orientation ~43 °, close to the value measured in cells not exposed to flow (Fig. 6C-E).

To relate abnormal polarization of lymphatic-valve-forming ECs in *Sdc4*$^{-/-}$ mice to a flow sensing defect, we tested the ability of LECs with reduced syndecan-4 expression to align under flow. Primary LECs were transfected with scrambled siRNA (siScrambled) or siRNA against *SDC4* (siSDC4) (Fig. S10A,B) and subjected to laminar flow (8 dynes/cm^2). After sixteen hours of flow exposure, control LECs (transfected with siScrambled) were elongated along the flow axis with phalloidin labeling demonstrating remodeling of actin fibers into long, fine filaments (Fig. 7B). In contrast, LECs transfected with siSDC4 (*SDC4* KD LECs) exhibited a cuboidal morphology with actin fibers in these cells retaining a thick and short appearance and, failed to align along the flow direction (Fig. 7B).

Measurements of cell orientation in response to laminar flow confirmed these observations. When subjected to flow, control LECs aligned to flow with the average orientation between 35 ° to 40 ° relative to flow direction (Fig. 7C, 1st set of bars). In contrast, flow had no effect on the alignment of *SDC4* KD cells. *SDC4* KD LECs showed an average orientation of ~45 ° which was similar to cells not subjected to flow (static) (Fig. 7C, 2nd set of bars). Remarkably, reducing VANGL2 levels in *SDC4* KD LECs restored their

ability to align under flow (Fig. 7B and Fig. 7C, 3rd set of bars). In fact, these cells aligned as well as control cells (Fig. 7B,C).

We also examined flow-mediated activation of VEGFR3 signaling in control and *SDC4* KD LECs (Fig. S10C). As expected, flow activated VEGFR3 signaling in control LECs (Fig. S10C). In contrast, flow-induced activation of VEGFR3 signaling was significantly reduced in *SDC4* KD cells (Fig. S10C).

DISCUSSION

The data presented in this study identify two new regulators of fluid shear stress-mediated lymphatic vasculature remodeling: Syndecan-4 and Pecam-1. A deletion of either gene in mice resulted in a similar lymphatic remodeling defect during embryonic development. Moreover, a simultaneous deletion of both genes caused a more severe lymphatic phenotype that included the appearance of blood-filled jugular lymph sac at E15.5. This phenotype is unlikely secondary to blood vessel defects as hemorrhage or other obvious blood vessel abnormalities were not seen in these animals. One potential explanation is the formation of abnormal lympho-venous valves resulting in blood backflow into the lymphatic vascular network. Another phenotype observed in *Sdc4*$^{-/-}$ or *Pecam-1*$^{-/-}$ was an increase in mural cell coverage in lymphatic vessels that was even more pronounced in *Sdc4*$^{-/-}$; *Pecam-1*$^{-/-}$ double nulls. These data support the idea of the existence of abnormal flow signaling in these mutants and is consistent with a previous report (Sweet et al., 2015). Enlarged lymphatic vessel diameter developed in *Sdc4*$^{-/-}$ has been linked with increased LEC proliferation. It is not the case in *Pecam-1* nulls. Although *Sdc4*$^{-/-}$ or some *Sdc4*$^{-/-}$*; Pecam1*$^{-/-}$ double knockout mice can survive till adulthood, the presence of abnormal lymphatic valves in adult mutants may affect the function of lymphatic vessels leading to increased morbidity (Alexander et al., 2010).

The more severe lymphatic phenotype developed in *Sdc4*$^{-/-}$; *Pecam-1*$^{-/-}$ double nulls suggests that syndecan-4 and Pecam-1 function through independent flow signaling pathways. While both have been implicated in flow signaling in LECs, the molecular mechanism involved are distinct: in the case of syndecan-4, it involves regulation of flow-mediated Vangl2 expression while PCP proteins do not seem to be involved in Pecam-1 controlled flow signaling (Fig. S11).

PECAM-1 involvement in mechanotransduction is well established in blood endothelial cells (BECs) where it transduces shear forces to activate a complex with VE-cadherin and VEGF receptor to mediate shear stress signaling (Tzima et al., 2005). However, its involvement in flow sensing events in the lymphatic endothelium has not been previously reported. A recent study has demonstrated that the transmembrane domain of VE-cadherin can bind directly to transmembrane domains of VEGFR2 and VEGFR3 (Coon et al., 2015), thus suggesting that VEGFR3, which is highly expressed in LECs, can be a part of a mechanotransduction complex. This is supported by the observation that changes in VEGFR3 levels in mice and zebrafish modulate aortic lumen diameter in a flow-dependent manner (Baeyens et al., 2015). The lymphatic remodeling defects observed in this study in *Pecam-1* knockout mice point to the importance of fluid shear stress-mediated signals in lymphatic vasculature development. The similar lymphatic abnormalities developed in *Sdc4*$^{-/-}$ and *Pecam-1*$^{-/-}$ mice suggest that the lymphatic vascular defects in *Sdc4* nulls are also due to impaired flow sensing in LECs.

While PECAM-1's role in flow sensing has been extensively investigated, relatively little is known about syndecan-4 involvement in this process. We recently demonstrated that aortic endothelial cells of *Sdc4* null mice are poorly aligned in the direction of flow and that *SDC4* knockdown in human umbilical vein endothelial cells inhibits flow-induced alignment, a defect rescued by re-expression of the gene (Baeyens et al., 2014).

Surprisingly, a PCP protein Vangl2 was identified as an important component of syndecan-4-dependent shear stress signals in this study. The laminar flow up-regulates VANGL2 expression in LECs *in vitro*, indicating that VANGL2 is a flow responsive gene. Consistent with this observation, we found that flow had only minimal effects on VANGL2 expression in *PECAM-1* KD LECs that are defective in transducing mechanical forces. However, in the setting of reduced syndecan-4 expression, exposure to flow led to a much higher increase in VANGL2 expression than what was seen in control LECs. Increased Vangl2 levels were also observed in lymphatic vessels in *Sdc4* null mice. These results suggest that syndecan-4 controls the extent of flow-induced increase in VANGL2 expression.

The excessive increase in VANGL2 expression in response to flow in LECs with reduced syndecan-4 expression accounts for the misalignment of these cells. Indeed, VANGL2 over-expression in control (WT) LECs impaired their ability to align to flow while the reduction of VANGL2 expression in *SDC4* KD LECs restored their ability to align. Combined with observations of abnormal lymphatic valve morphogenesis in *Vangl2*-deficient mice (Tatin et al., 2013), these data suggest that there is an optimal level of Vangl2 expression in LECs. The concept of the optimal expression level of a particular protein with regard to the regulation of flow-mediated cell alignment is consistent with a recent description of an endothelial flow-sensing set-point study (Baeyens et al., 2015).

The involvement of PCP proteins in lymphatic valve morphogenesis has been previously reported. Ablation of core PCP proteins Celsr1 or Vangl2 in mice results in formation of abnormal lymphatic valves due to a reorientation defect of lymphatic-valve-forming cells (Tatin et al., 2013). Moreover, Vangl2 has been shown to be involved in flow-controlled ependymal cilia orientation (Guirao et al., 2010), suggesting that this PCP protein plays a role in integration of fluid shear stress-mediated signals. Yet how it achieves this effect remains unknown. Our results expand this concept by demonstrating that *VANGL2* is a flow

responsive gene and its expression levels induced by flow are critical for LECs to align to flow. We have further identified that syndecan-4 is an important regulator in this process.

The need for the optimal Vangl2 level controlling cell orientation is consistent with what is known about PCP protein involvement in cell polarization. In vertebrate inner ear hair cell, core PCP proteins Frizzled (Fz) and Dishevelled (Dvl) form a complex on one side of the cell that is opposite to Van Gogh (Vangl) and Prickle (Pk) on the other. This asymmetric distribution of the PCP proteins is required for hair cell polarization (Deans et al., 2007; Etheridge et al., 2008; Montcouquiol et al., 2006; Wang et al., 2006; Yin et al., 2012). Increased Vangl2 levels in *Sdc4*$^{-/-}$ LECs may disrupt PCP protein distribution in the cells resulting in abnormal cellular orientation.

The appearance of "wavy" endothelial cell-cell junctions in the lymphatic vessels of *Sdc4*$^{-/-}$ mice is consistent with a degree of destabilization. Indeed, the involvement of PCP proteins in controlling classical cadherins has previously been reported (Nagaoka et al., 2014a; Nagaoka et al., 2014b). In the nervous system, Vangl2 binds directly to the intracellular domain of N-cadherin to stabilize cell-cell junctions (Nagaoka et al., 2014b). Similarly, Vangl2 controls E-cadherin in epithelial cells (Nagaoka et al., 2014a). It is, therefore, likely that in LECs, Vangl2 binds VE-cadherin to regulate the formation of endothelial adherens junctions.

In summary, our study has identified a new mechanism of fluid shear stress-mediated signaling that involves syndecan-4-dependent up-regulation of the PCP protein Vangl2 driven by flow.

MATERIALS AND METHODS

Mice

Sdc4$^{-/-}$ and *Pecam-1*$^{-/-}$ strains are maintained in C57Bl/6J background. *Sdc4*$^{-/-}$; *Pecam-1*$^{-/-}$ mouse was generated by breeding *Sdc4*$^{+/-}$; *Pecam-1*$^{-/-}$ with *Sdc4*$^{+/-}$; *Pecam-1*$^{-/-}$. The morning that vaginal plug is found is designated as embryonic stage (E)0.5.

Whole-mount immunofluorescence staining and image acquisition

For whole-mount immunofluorescence staining of mesentery, tissue was fixed in 1 % PFA for 1 hour at room temperature (RT) followed by washed with ice-cold PBS for 3 times. Tissue was blocked in blocking buffer containing 5 % donkey serum, 0.2 % BSA, 0.3 % Triton X-100 in PBS for 1 hour at RT before incubated with primary antibody diluted in blocking buffer overnight at room temperature. After washed with wash buffer containing 0.3 % Triton X-100 in PBS, tissue was incubated with secondary antibody diluted in blocking buffer at 4 degrees. Next day, tissue was washed with wash buffer and flat mounted using fluorescent mounting medium (DAKO). Images were acquired using Leica DM6000 CS confocal microscope or Nikon Eclipse 80i. Confocal images are maximum intensity projections of confocal z stacks. Nuclear orientation and shape (roundness) of Prox1^{high} valve-forming ECs were quantified using ImageJ.

Antibodies used for whole-mount immunofluorescence staining

Primary antibodies: Rabbit anti-Prox1 (#11002, AngioBio, 1:200), Rabbit anti-Lyve1 (#11-034, AngioBio, 1:400), rabbit anti-Laminin-α5 (Ringelmann et al., 1999, 1:1000), rat anti-VE-cadherin (Clone 11D4.1, #555289, BD Biosciences, 1:100), goat anti-Vegfr3 (AF743, R&D Systems, 1:100), hamster anti-podoplanin (Hybridoma Bank, Developmental Studies, University of Iowa, 1:1000), Cy3-conjugated α-SMA (Clone 1A4, #C6198, Sigma-Aldrich,

1:400), and Alexa fluor 488-conjugated phalloidin (#A12379, Life Technologies, 1:200). Secondary antibodies: Alexa 647-conjugated chicken anti-rabbit (A-21443, Invitrogen, 1:200), Alexa 594-conjugated chicken anti-rabbit (A-21442, Invitrogen, 1:200), Alexa 488-conjugated chicken anti-goat (A21467, Invitrogen, 1:200), Alexa 488-conjugated donkey anti-rat (A-21208, Invitrogen, 1:200), and Alexa 647-conjugated goat anti-hamster (A21451, Invitrogen, 1:200).

Cell culture and siRNA transfection

LECs used in this study are hDLECs (Lonza, CC-2812) which were cultured in EGM-2MV media (Lonza, CC-3202). For gene KD in LECs, cells were transfected with siRNAs using Lipofectamine RNAiMAX (Invitrogen) *according* to the *manufacturer*'s *instructions.* siRNA was washed out 6-8 hours after transfection. Transfected cells were harvested for experiments 72 hours after transfection.

siRNA used for gene KD: Scrambled siRNA (OriGene Technologies), siRNA against human SDC4 (OriGene Technologies, SR304301), siRNA against human VANGL2 (OriGene Technologies, SR311428), and siRNA against human PECAM-1 (15nM) (OriGene Technologies, SR303439).

Lentiviral transduction

LECs were transduced with lentiviral particles expressing control (OHS5833, GE Healthcare Dharmacon) or VANGL2 (OHS5899-202624111, analysis). Protein expression was identified by immunoblot analysis.

qRT-PCR analysis

1µg of RNA was used for cDNA synthesis using Superscript III First-Strand Synthesis System (Invitrogen) following the manufacturer's instructions. 3ul cDNA was used for each qPCR reaction, which was performed in a 25µl reaction volume in triplicate. qPCR analysis was performed on CFX96 Real-Time System C1000 Thermal Cycler (Bio-Rad) using iQ SYBR® Green Supermix (Bio-Rad). Four independent experiments were carried out.

Program for qPCR amplification: PCR amplification using an initial denaturation step at 95°C for 10 minutes, followed by 40 cycles of PCR at 95°C for 15 seconds and 60°C for 1 minute.

qPCR primers: Primers for VANGL2 were purchased from QIAGEN (PPH12377B-200). Sequences for other primers are as follow:

Vangl2 Forward: 5' ccagccgcttctacaatgtc 3'

Vangl2 Reverse: 5' tctccaggatccacactgc 3'

Celsr1 Forward: 5' ggcagtcatgaccttggacta 3'

Celsr1 Reverse: 5' agctgattcccaatctgcac 3'

Mouse syndecan-4 Forward: 5' catctttgagagaactgaggtcttg 3'

Mouse syndecan-4 Reverse: 5' ccttcttcttcatgcggtaca 3'

Pecam-1 Forward: 5' cggtgttcagcgagatcc 3'

Pecam-1 Reverse: 5' actcgacaggatggaaatcac 3'

18S rRNA Forward: 5' aggaattcccagtaagtgcg 3'

18S rRNA Reverse: 5' gcctcactaaaccatccaa 3'

ACTB Forward: 5' ccaaccgcgagaagatga 3'

ACTB Reverse: 5' ccagaggcgtacagggatag 3'

Human syndecan-4 Forward: 5' ggcaggaatctgatgactttg 3'

Human syndecan-4 Reverse: 5’ gccgatcatggagtcttcc 3’

CELSR1 Forward: 5’ tggatatctccaggcgtga 3’

CELSR1 Reverse: 5’ agcggcataggtgacaatct 3’

Isolation of total RNA from thoracic duct

Thoracic ducts were dissected out from 10 adult wildtype and *Sdc4*$^{-/-}$ mice, respectively, and were collected in Buffer RLT Plus (RNeasy Plus Lysis Buffer, QIAGEN). Tissue was homogenized using TissueLyser II (QIAGEN) followed by spining down at 4°C. Supernatant was collected, from which total RNA was extracted using RNeasy Plus Mini Kit (QIAGEN).

Flow-Assisted Cell Sorting

Mesenteric vessels of E18.5 control, *Sdc4*$^{-/-}$ or *Pecam-1*$^{-/-}$ embryos were digested for 30 minutes at 37ºC in 1mg/mL collagenase type II with periodic gentle inversion to mix, followed by mechanical dissociation via repeated pipetting. Single cells were incubated in 10µg/mL Hoechst 3342 (Sigma) for 30 minutes at 37ºC, followed by an additional 15 minute incubation with 0.5µg/mL Pyronin Y (Sigma) and fluorescently conjugated antibodies CD31-FITC, CD144-FITC, CD45-PECy7, and Lyve1-Alexa647. Endothelial cells were identified as events negative for CD45 and positive for either CD31 (*Sdc4*$^{-/-}$ experiments) or CD144 (*Pecam-1*$^{-/-}$ experiments) endothelial markers; lymphatic endothelial cells were subsequently discriminated as Lyve1+. Two-dimensional cell cycle FACS analysis was then performed on blood and lymphatic endothelial cell events by comparing DNA (Hoechst) and RNA (Pyronin Y) content.

Western blotting analysis

Cells were rapidly washed with ice-cold PBS twice and lysed with 100 µl RIPA lysis buffer containing complete mini EDTA-free protease inhibitors (#11836170001, Roche) and phosphatase inhibitors (#04906837001, Roche). Cell lysates were subjected to two cycles of snap-freezing in liquid nitrogen and then cleared by spin down at 15,000 rpm for 10 minutes. Protein concentration was determined using BCA protein assay (Thermo Scientific) and equalized in each sample. Forty micrograms of total protein from each sample were loaded onto a 4–15 % TGX gel (Bio-Rad) with Tris/Glycine/SDS Buffer (Bio-Rad) for SDS-PAGE separation and transferred to an Immobilon-P Transfer Membrane (PVDF) (IPVH 00010, Millipore). Membranes were blocked with 5 % non-fat dry milk (AB 10109-01000, AmericanBio) in Tris-buffered saline containing 0.05 % Tween20 (TBS-T) for 1 hour at room temperature and then incubated with primary antibodies at 4°C overnight. Membranes were washed with TBS-T and incubated with secondary antibodies for 2 hours at room temperature. Protein bands were visualized using HRP-conjugated secondary antibodies associated to enhanced chemiluminescence (Immobilon Western Chemiluminescent HRP Substrate, WBKL S0500, Millipore). Signals from chemiluminescent reaction were recorded using a digital acquisition system (G-Box, Syngene) equipped with a 1.4-megapixel charge-coupled device (CCD) camera with a “true” 1.4-megapixel resolution.

Primary antibodies: anti-syndecan 4 (abcam, ab24511, 1:1000), anti-Actin (Santacruz, sc-1615, 1:200), anti-VANGL2 (R&D systems, AF4815, 1:100), Anti-VEGFR3 (Cell Signaling Technology, #2638, 1:1000), Anti-Phospho-VEGFR3 (Cell Applications, INC. cy1115, 1:1000), Anti-β-Actin (Sigma, A1978, 1:10000). Secondary antibodies: peroxidase labeled goat anti-rabbit IgG (Vector Laboratories, PI-1000, 1:5000), peroxidase labeled horse anti-goat IgG (Vector Laboratories, PI-9500, 1:5000), peroxidase labeled rabbit anti-sheep IgG

(Thermo Scientific, #31480, 1:5000), peroxidase labeled horse anti-mouse IgG (Vector Laboratories, PI-2000, 1:5000).

Shear stress

LECs were seeded on fibronectin-coated (20 μg/ml) tissue culture plastic slides. After reaching confluency, cells were starved with EBM-2 medium (Lonza, CC-3156) containing 5 % FBS, 100 U/mL penicillin and 100 μg/mL streptomycin for 4 hours. Shear stress with a calculated intensity of 8 dynes/cm^2 was applied in a parallel flow chamber with starvation medium. After 16 or 20 hours of steady laminar flow, cell alignment was quantified by measuring the nuclear orientation using a custom made Matlab function (Baeyens et al., 2014). ≥ 50 images/condition/experiment taken under 20x objective were used for quantification.

Statistical analysis

GraphPad Prism 6 was used for statistical analysis. Student's t-test (two-tailed), Mann-Whitney test, Kruskal-Wallis test, one-way ANOVA, and 2way ANOVA were applied to determine statistical significance.

Study approval

All mouse experiments were complied with protocols approved by Yale University Institutional Animal Care and Use Committee.

Acknowledgements

We thank Eleni Tzima for *Pecam-1*$^{-/-}$ mice, Anne Eichmann for helpful discussion, Lydia Sorokin for Laminin-a5 antibody and Gyong Ju Min for help with flow experiment.

Competing interests

The authors declare no competing or financial interests.

Author contributions

Y.W. carried out most of the experiments and prepared figures. N.B. conducted flow experiments and quantified the shape and the orientation of lymphatic-valve-forming cells. F.C. performed western blotting. K.T. conducted flow experiments and western blotting. J.F. performed FACS. J.Z. isolated thoracic ducts from mice. Y.J. and D.L. helped with analysis of lymphatic phenotypes. B.C. helped with flow experiment. K.H. and M.A.S. helped with data analysis, study design and manuscript preparation. Y.W. and M.S. designed the project and wrote the manuscript. M.S. supervised all aspects of the project.

Funding

This work was supported by the National Institutes of Health [R01 HL062289 to M.S., R01 HL075092 to M.A.S., R01 HL128064 to K.H.], American Heart Association Postdoctoral Fellowship [14POST19020010 to N.B.] and Borsa di studio SIF-MSD Italia [to F.C.].

References

Alexander, J., Ganta, V.C., Jordan, P., Witte, M.H., 2010. Gastrointestinal lymphatics in health and disease. Pathophysiology 17, 315-335.

Astudillo, P., Carrasco, H., Larraín, J., 2014. Syndecan-4 inhibits Wnt/β-catenin signaling through regulation of low-density-lipoprotein receptor-related protein (LRP6) and R-spondin 3. The international journal of biochemistry & cell biology 46, 103-112.

Baeyens, N., Mulligan-Kehoe, M.J., Corti, F., Simon, D.D., Ross, T.D., Rhodes, J.M., Wang, T.Z., Mejean, C.O., Simons, M., Humphrey, J., 2014. Syndecan 4 is required for endothelial alignment in flow and atheroprotective signaling. Proceedings of the National Academy of Sciences 111, 17308-17313.

Baeyens, N., Nicoli, S., Coon, B.G., Ross, T.D., Van den Dries, K., Han, J., Lauridsen, H.M., Mejean, C.O., Eichmann, A., Thomas, J.-L., 2015. Vascular remodeling is governed by a VEGFR3-dependent fluid shear stress set point. Elife 4, e04645.

Bellin, R.M., Kubicek, J.D., Frigault, M.J., Kamien, A.J., Steward, R.L., Barnes, H.M., DiGiacomo, M.B., Duncan, L.J., Edgerly, C.K., Morse, E.M., 2009. Defining the role of syndecan-4 in mechanotransduction using surface-modification approaches. Proceedings of the National Academy of Sciences 106, 22102-22107.

Chen, C.-Y., Bertozzi, C., Zou, Z., Yuan, L., Lee, J.S., Lu, M., Stachelek, S.J., Srinivasan, S., Guo, L., Vincente, A., 2012. Blood flow reprograms lymphatic vessels to blood vessels. The Journal of clinical investigation 122, 2006-2017.

Coon, B.G., Baeyens, N., Han, J., Budatha, M., Ross, T.D., Fang, J.S., Yun, S., Thomas, J.-L., Schwartz, M.A., 2015. Intramembrane binding of VE-cadherin to VEGFR2 and VEGFR3 assembles the endothelial mechanosensory complex. The Journal of cell biology 208, 975-986.

Deans, M.R., Antic, D., Suyama, K., Scott, M.P., Axelrod, J.D., Goodrich, L.V., 2007. Asymmetric distribution of prickle-like 2 reveals an early underlying polarization of vestibular sensory epithelia in the inner ear. The Journal of neuroscience 27, 3139-3147.

Elfenbein, A., Lanahan, A., Zhou, T.X., Yamasaki, A., Tkachenko, E., Matsuda, M., Simons, M., 2012. Syndecan 4 Regulates FGFR1 Signaling in Endothelial Cells by Directing Macropinocytosis. Science signaling 5, ra36.

Elfenbein, A., Simons, M., 2013. Syndecan-4 signaling at a glance. J Cell Sci 126, 3799-3804.

Escobedo, N., Contreras, O., Muñoz, R., Farías, M., Carrasco, H., Hill, C., Tran, U., Pryor, S.E., Wessely, O., Copp, A.J., 2013. Syndecan 4 interacts genetically with Vangl2 to regulate neural tube closure and planar cell polarity. Development 140, 3008-3017.

Etheridge, S.L., Ray, S., Li, S., Hamblet, N.S., Lijam, N., Tsang, M., Greer, J., Kardos, N., Wang, J., Sussman, D.J., 2008. Murine dishevelled 3 functions in redundant pathways with dishevelled 1 and 2 in normal cardiac outflow tract, cochlea, and neural tube development. PLoS Genet 4, e1000259.

Finsen, A.V., Lunde, I.G., Sjaastad, I., Østli, E.K., Lyngra, M., Jarstadmarken, H.O., Hasic, A., Nygård, S., Wilcox-Adelman, S.A., Goetinck, P.F., 2011. Syndecan-4 is essential for development of concentric myocardial hypertrophy via stretch-induced activation of the calcineurin-NFAT pathway. PloS one 6, e28302.

Guirao, B., Meunier, A., Mortaud, S., Aguilar, A., Corsi, J.-M., Strehl, L., Hirota, Y., Desoeuvre, A., Boutin, C., Han, Y.-G., 2010. Coupling between hydrodynamic forces and planar cell polarity orients mammalian motile cilia. Nature Cell Biology 12, 341-350.

Horowitz, A., Tkachenko, E., Simons, M., 2002. Fibroblast growth factor-specific modulation of cellular response by syndecan-4. J Cell Biol 157, 715-725.
Montcouquiol, M., Sans, N., Huss, D., Kach, J., Dickman, J.D., Forge, A., Rachel, R.A., Copeland, N.G., Jenkins, N.A., Bogani, D., 2006. Asymmetric localization of Vangl2 and Fz3 indicate novel mechanisms for planar cell polarity in mammals. The Journal of neuroscience 26, 5265-5275.
Muñoz, R., Moreno, M., Oliva, C., Orbenes, C., Larraín, J., 2006. Syndecan-4 regulates non-canonical Wnt signalling and is essential for convergent and extension movements in Xenopus embryos. Nature cell biology 8, 492-500.
Nagaoka, T., Inutsuka, A., Begum, K., Kishi, M., 2014a. Vangl2 regulates E-cadherin in epithelial cells. Scientific reports 4, 6940.
Nagaoka, T., Ohashi, R., Inutsuka, A., Sakai, S., Fujisawa, N., Yokoyama, M., Huang, Y.H., Igarashi, M., Kishi, M., 2014b. The Wnt/planar cell polarity pathway component Vangl2 induces synapse formation through direct control of N-cadherin. Cell reports 6, 916-927.
Ohkawara, B., Glinka, A., Niehrs, C., 2011. Rspo3 binds syndecan 4 and induces Wnt/PCP signaling via clathrin-mediated endocytosis to promote morphogenesis. Developmental cell 20, 303-314.
Sabine, A., Agalarov, Y., Maby-El Hajjami, H., Jaquet, M., Hägerling, R., Pollmann, C., Bebber, D., Pfenniger, A., Miura, N., Dormond, O., 2012. Mechanotransduction, PROX1, and FOXC2 cooperate to control connexin37 and calcineurin during lymphatic-valve formation. Developmental cell 22, 430-445.
Sabine, A., Bovay, E., Demir, C.S., Kimura, W., Jaquet, M., Agalarov, Y., Zangger, N., Scallan, J.P., Graber, W., Gulpinar, E., 2015. FOXC2 and fluid shear stress stabilize postnatal lymphatic vasculature. The Journal of clinical investigation 125, 3861.
Sweet, D.T., Jiménez, J.M., Chang, J., Hess, P.R., Mericko-Ishizuka, P., Fu, J., Xia, L., Davies, P.F., Kahn, M.L., 2015. Lymph flow regulates collecting lymphatic vessel maturation in vivo. The Journal of clinical investigation 125, 2995-3007.
Tatin, F., Taddei, A., Weston, A., Fuchs, E., Devenport, D., Tissir, F., Makinen, T., 2013. Planar cell polarity protein Celsr1 regulates endothelial adherens junctions and directed cell rearrangements during valve morphogenesis. Developmental cell 26, 31-44.
Tzima, E., Irani-Tehrani, M., Kiosses, W.B., Dejana, E., Schultz, D.A., Engelhardt, B., Cao, G., DeLisser, H., Schwartz, M.A., 2005. A mechanosensory complex that mediates the endothelial cell response to fluid shear stress. Nature 437, 426-431.
Wang, Y., Guo, N., Nathans, J., 2006. The role of Frizzled3 and Frizzled6 in neural tube closure and in the planar polarity of inner-ear sensory hair cells. The Journal of neuroscience 26, 2147-2156.
Yin, H., Copley, C.O., Goodrich, L.V., Deans, M.R., 2012. Comparison of phenotypes between different vangl2 mutants demonstrates dominant effects of the Looptail mutation during hair cell development. PLoS One 7, e31988.

Figures

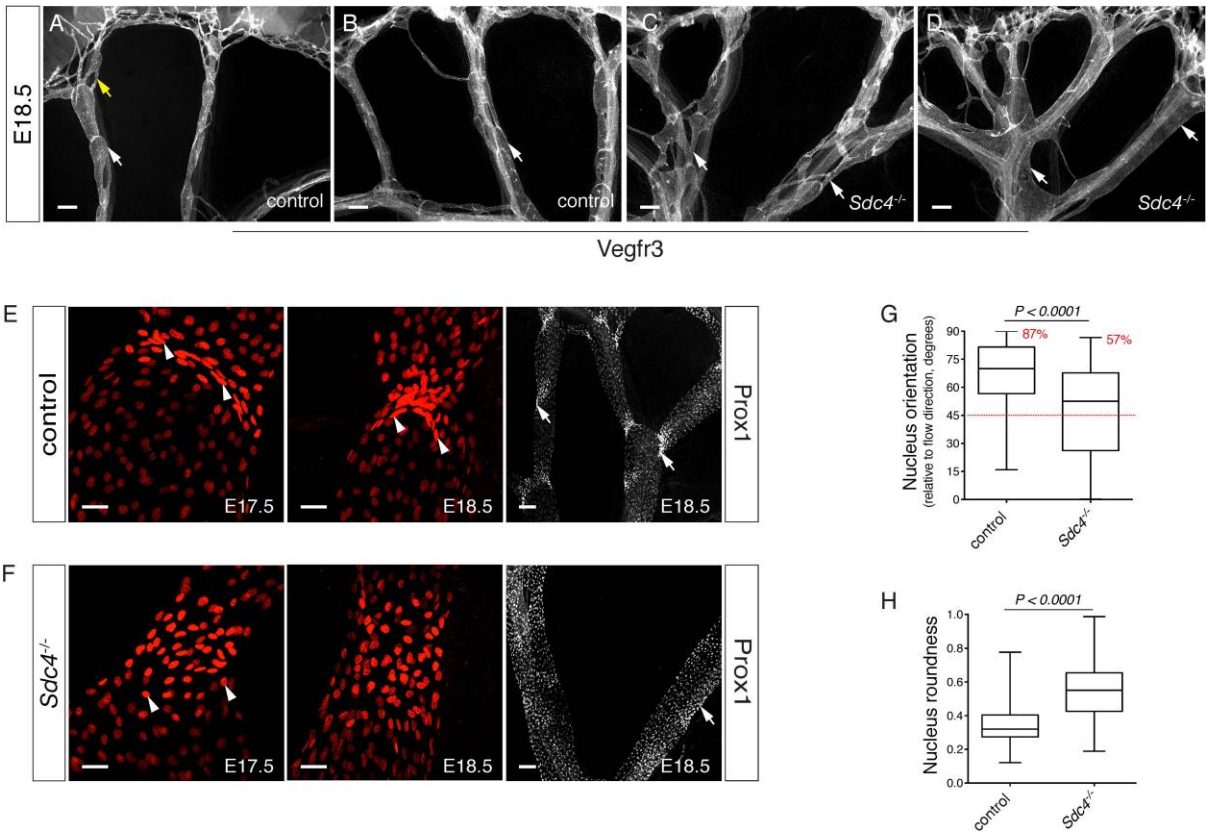

Fig. 1. Lymphatic vessels show remodeling defects in *Sdc4*$^{-/-}$ mice during late embryonic development. (A-D) Whole-mount immunofluorescence staining for VEGFR3 showing a hierarchal lymphatic vascular network developed in the mesentery in control mice at E18.5 (A-B, arrows). In *Sdc4* nulls, lymphatic vessels are abnormally branched and tend to form a vascular plexus (C, arrows). Enlarged lymphatic vessels were also seen in *Sdc4*$^{-/-}$ mice (D, arrows). Scale bars: 200um. (E) Prox1^{high} lymphatic-valve-forming ECs reorient perpendicular to flow direction at E17.5 in control animals. Note, the nuclei of valve-forming cells are highly elongated and are tightly packed (left, arrowheads). At E18.5, valve-forming cells reorganize again and form mature lymphatic valves containing two leaflets (middle, arrowheads). Prox1^{high} valve-forming cells are concentrated in valve areas in control (right, arrows). Scale bars: left, middle, 30um; right, 100um. (F) The nuclei of Prox1^{high} valve-forming cells are rounded (left, arrowheads), randomly oriented (left), and are loosely

arranged (left) in *Sdc4*$^{-/-}$ mice at E17.5. Nuclei with similar morphology and organization were also seen in the mutants at E18.5 (middle). Some of the Prox1^{high} valve-forming cells in *Sdc4*$^{-/-}$ do not reorient, and are remained parallel to the longitudinal axis of lymphatic vessels (right, arrow). Scale bars: left, middle, 30um; right, 100um. (G) Nuclear orientation of Prox1^{high} cells in E17.5 mesenteric lymphatic vessels of control and *Sdc4*$^{-/-}$ mice (n = 5). The percentage of nuclei reoriented >45 ° relative to flow direction is indicated. Mann-Whitney test. (H) Quantification of nuclear shape (roundness) of Prox1^{high} cells in E17.5 mesenteric lymphatic vessels (n = 5). Mann-Whitney test.

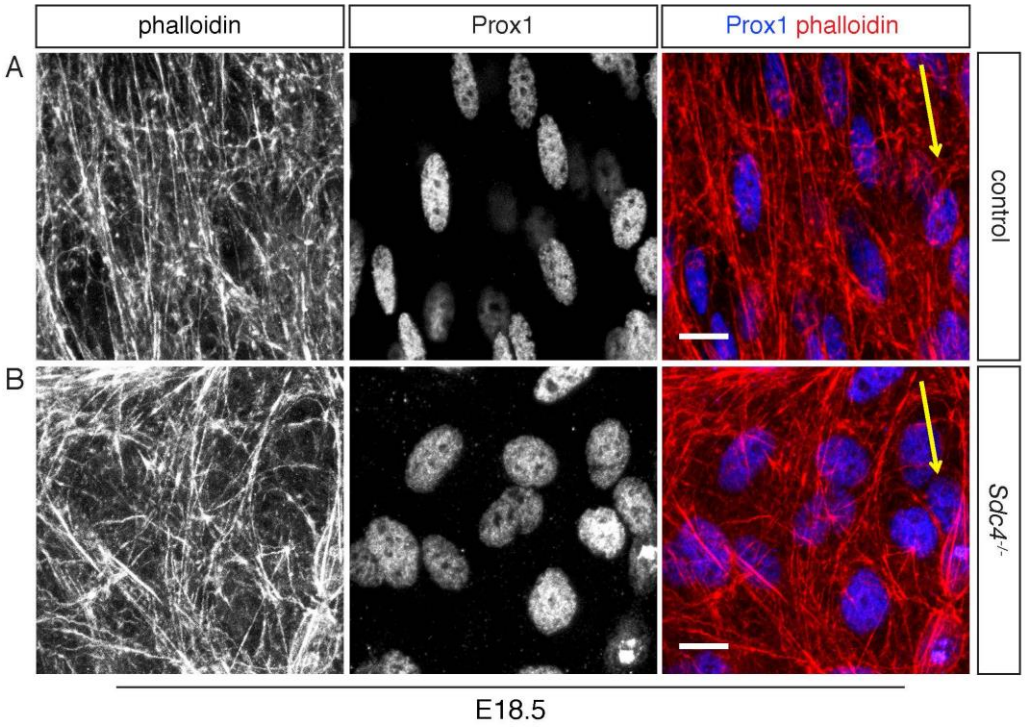

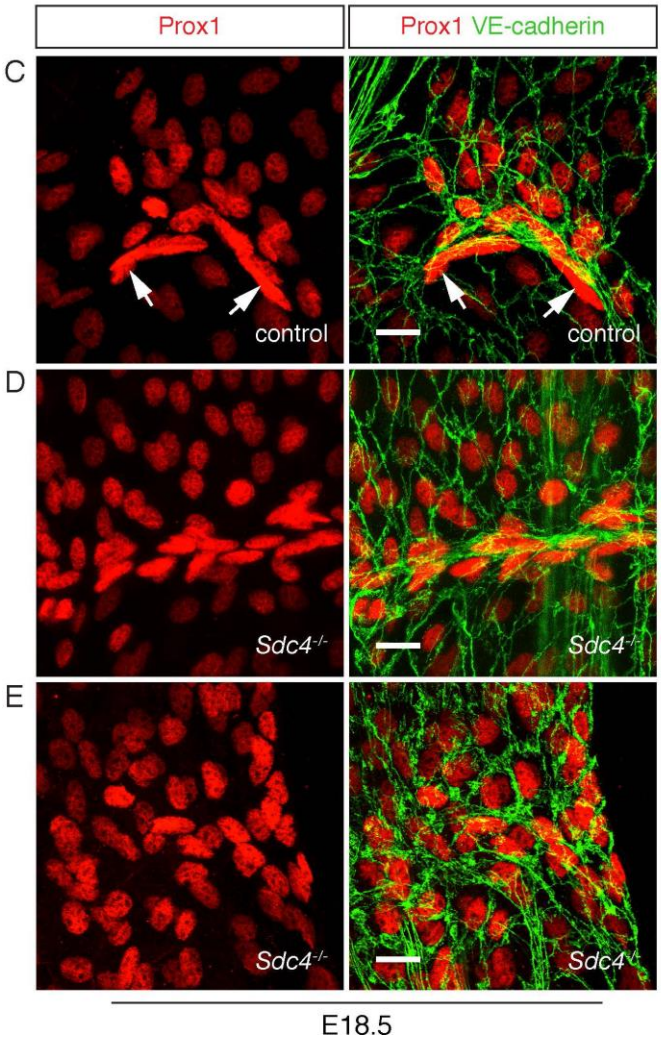

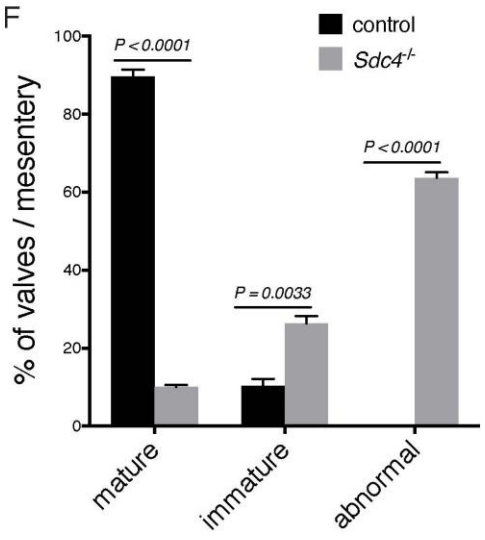

Fig. 2. Abnormal alignment of actin filaments and compromised formation of lymphatic valves in *Sdc4* null mice. (A) Phalloidin labeling showing long, fine actin fibers of LECs align to flow direction in control animals. Scale bar: 10um. Yellow arrow indicates flow direction in lymphatic vessel. (B) In *Sdc4* nulls, actin filaments are thick, short and randomly organized. Scale bar: 10um. Yellow arrow indicates flow direction in lymphatic vessel. (C) Representative images of V-shape mature lymphatic valves in control mice (arrows). Scale bar: 15um. (D-E) Ring-shape, immature lymphatic valves (D) and abnormal valves consisting of randomly oriented Prox1^{high} lymphatic-valve-forming ECs (E) in *Sdc4*$^{-/-}$ animals. Scale bar: 15um. (F) Quantification of lymphatic valves formed in mesentery at E18.5 based on Prox1 and VE-cadherin staining. The proportion (%) of different types of valves relative to the total number of valves formed per mesentery is shown. V-shape valves are defined as mature valves. Immature valves exhibit a ring-shape structure. Valves consisting of randomly organized Prox1^{high} valve-forming ECs or Prox1^{high} cells remaining parallel to flow direction are considered as abnormal valves. Student's t-test (two-tailed). Data are mean ± SEM (n = 3).

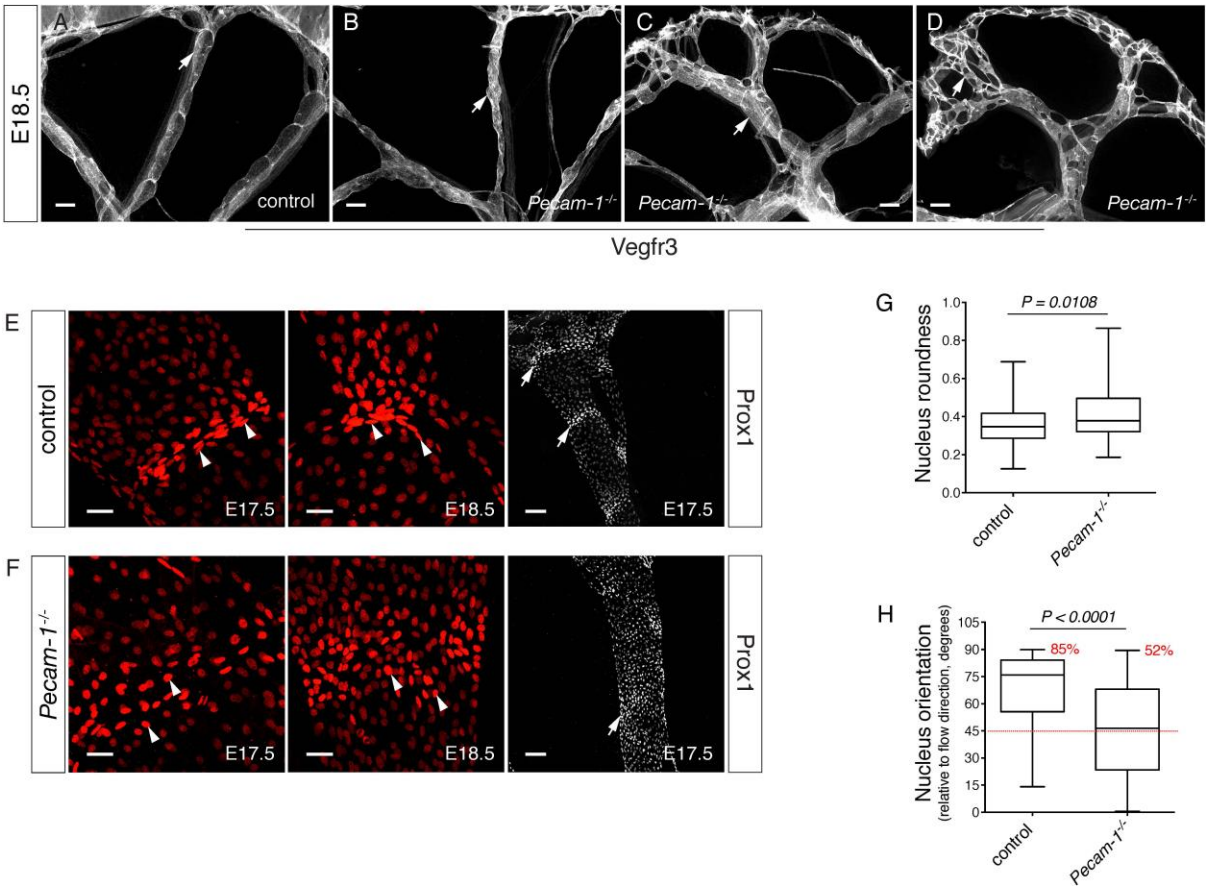

Fig. 3. *Pecam-1*$^{-/-}$ mice show lymphatic remodeling defects at E18.5. (A-D) Irregular (B, arrow), enlarged (C, arrow) and abnormally branched (D, arrow) mesenteric lymphatic vessels developed in *Pecam-1*$^{-/-}$ mice but not in controls (A, arrow) at E18.5. Scale bars: 200um. (E-F) Compared to control (E, left, middle, arrowheads), the nuclei of Prox1^{high} valve-forming cells in *Pecam-1*$^{-/-}$ are less elongated (F, left, middle, arrowheads), randomly oriented (F, left, middle) and are loosely organized (F, left, middle). Nuclei of Prox1^{high} valve-forming cells aligned along longitudinal axis of lymphatic vessels were also seen in *Pecam-1*$^{-/-}$ (F, right, arrow). In control mice, the nuclei of Prox1^{high} valve-forming cells are concentrated in valve areas (E, right, arrows). Scale bars: left, middle, 30um; right, 100um. (G) Quantification of nuclear shape (roundness) of Prox1^{high} cells in E17.5 mesenteric lymphatic vessels (n = 5). Mann-Whitney test. (H) Nuclear orientation of Prox1^{high} cells in

E17.5 mesenteric lymphatic vessels (n = 5). The percentage of nuclei reoriented >45 ° relative to flow direction is indicated. Mann-Whitney test.

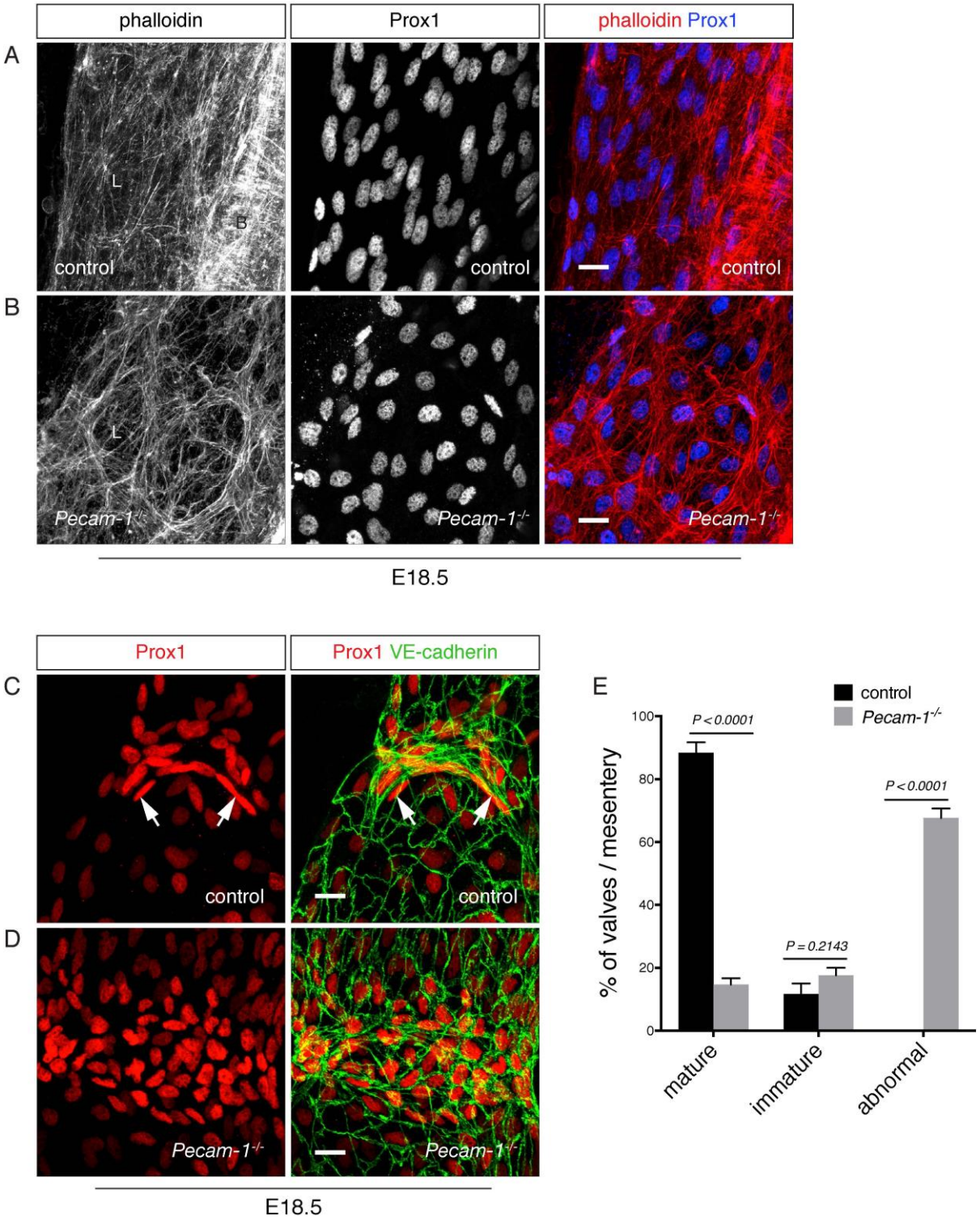

Fig. 4. Disorganized actin stress fibers and reduced formation of mature lymphatic valves in *Pecam-1*$^{-/-}$ mice at E18.5. (A) Long, fine actin filaments labeled by phalloidin align

to flow direction in lymphatic vessels (Prox1+) in control mice. Scale bar: 15um. B = blood vessel. L = lymphatic vessel. (B) In *Pecam-1*$^{-/-}$, actin fibers exhibit short, thick appearance, and do not align. Scale bar: 15um. L = lymphatic vessel. (C) Immunofluorescence staining showing V-shape mature lymphatic valves (arrows) developed in the mesentery in control mice. Scale bar: 15um. (D) Abnormal lymphatic valves containing randomly oriented Prox1^{high} valve-forming ECs were observed in *Pecam-1* knockouts. Scale bar: 15um. (E) Quantification of lymphatic valves formed in E18.5 mesentery based on staining for Prox1 and VE-cadherin. The proportion (%) of different types of valves relative to the total number of valves formed per mesentery is shown. Mature valves = V-shape; immature valves = ring shape; abnormal valves = valves consisting of randomly organized Prox1^{high} valve-forming cells or Prox1^{high} valve-forming cells aligned parallel to the longitudinal axis of lymphatic vessels. Student's t-test (two-tailed). Data represent mean ± SEM (n = 3).

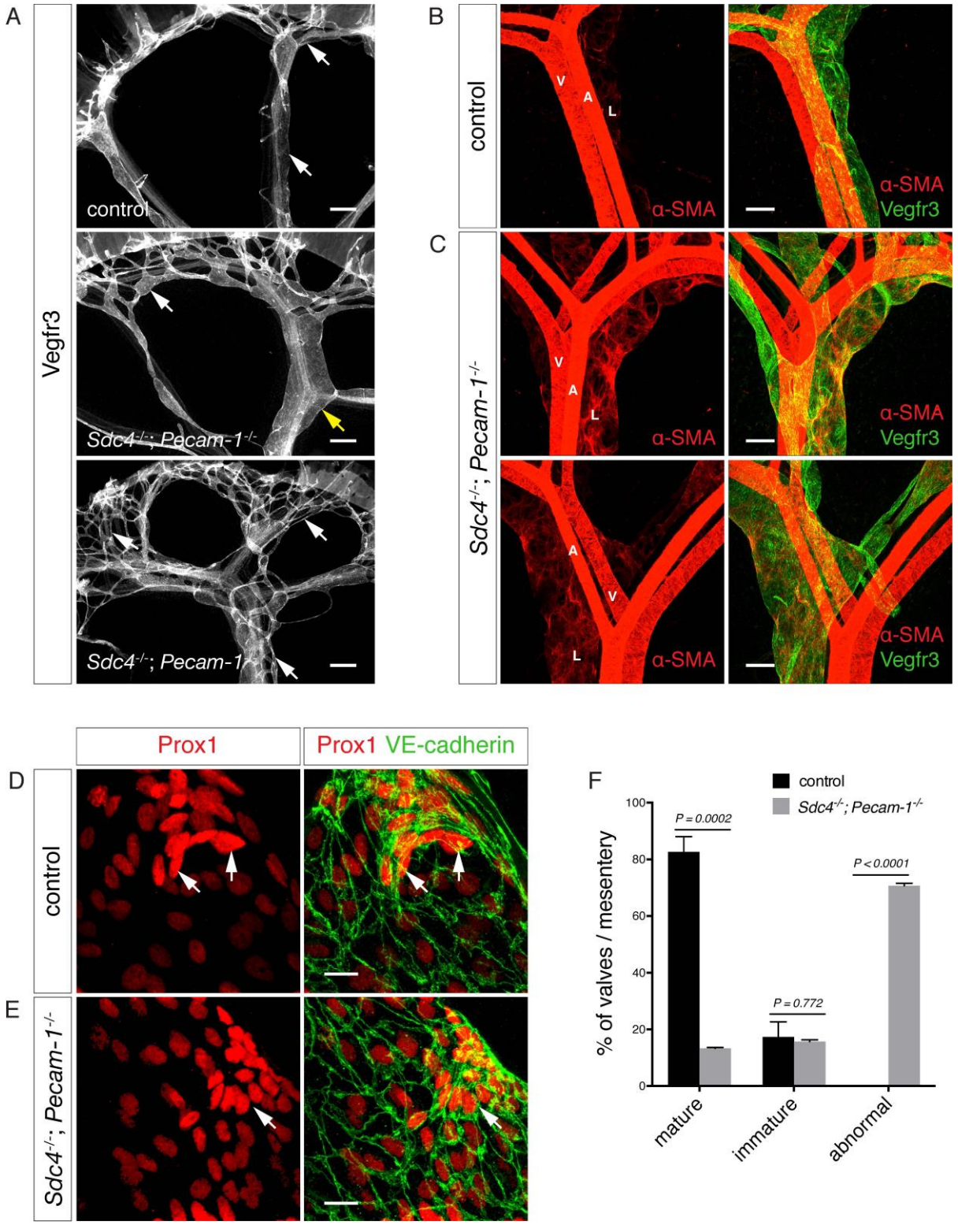

Fig. 5. *Sdc4*$^{-/-}$; *Pecam-1*$^{-/-}$ double nulls show severe lymphatic phenotype.

(A) Mesenteric lymphatic vessels in *Sdc4*$^{-/-}$; *Pecam-1*$^{-/-}$ embryos show irregular morphology (middle, white arrow), increased diameter (middle, yellow arrow) and abnormal branching (bottom, arrows) at E18.5, which were not seen in controls (upper, arrows). Scale bars: 200um. (B, C) Sparse mural cell (α-SMA+) coverage in mesenteric lymphatic vessels in control mice at E18.5 (B). Extensive mural cell recruitment in lymphatic vessels of *Sdc4*$^{-/-}$; *Pecam-1*$^{-/-}$ double nulls (C). A = artery, V = vein, L = lymphatic vessel. Scale bars: 100um. (D) Mature V-shape valves developed in mesenteric lymphatic vessels in control mice at E18.5 (arrows). Scale bar: 15um. (E) Abnormal lymphatic valves containing randomly oriented Prox1^{high} valve-forming ECs formed in *Sdc4*$^{-/-}$; *Pecam-1*$^{-/-}$ mice at E18.5 (arrows). Scale bar: 15um. (F) Quantification of lymphatic valves developed in the mesentery of control and *Sdc4*$^{-/-}$; *Pecam-1*$^{-/-}$ mice at E18.5 according to antibody staining against Prox1 and VE-cadherin. The proportion (%) of different types of valves relative to the total number of valves formed per mesentery is shown. Mature valves = V-shape; immature valves = ring shape; abnormal valves = valves consisting of randomly organized Prox1^{high} valve-forming cells or Prox1^{high} cells aligned parallel to the longitudinal axis of lymphatic vessels. Student's t-test (two-tailed). Data represent mean ± SEM (n = 3).

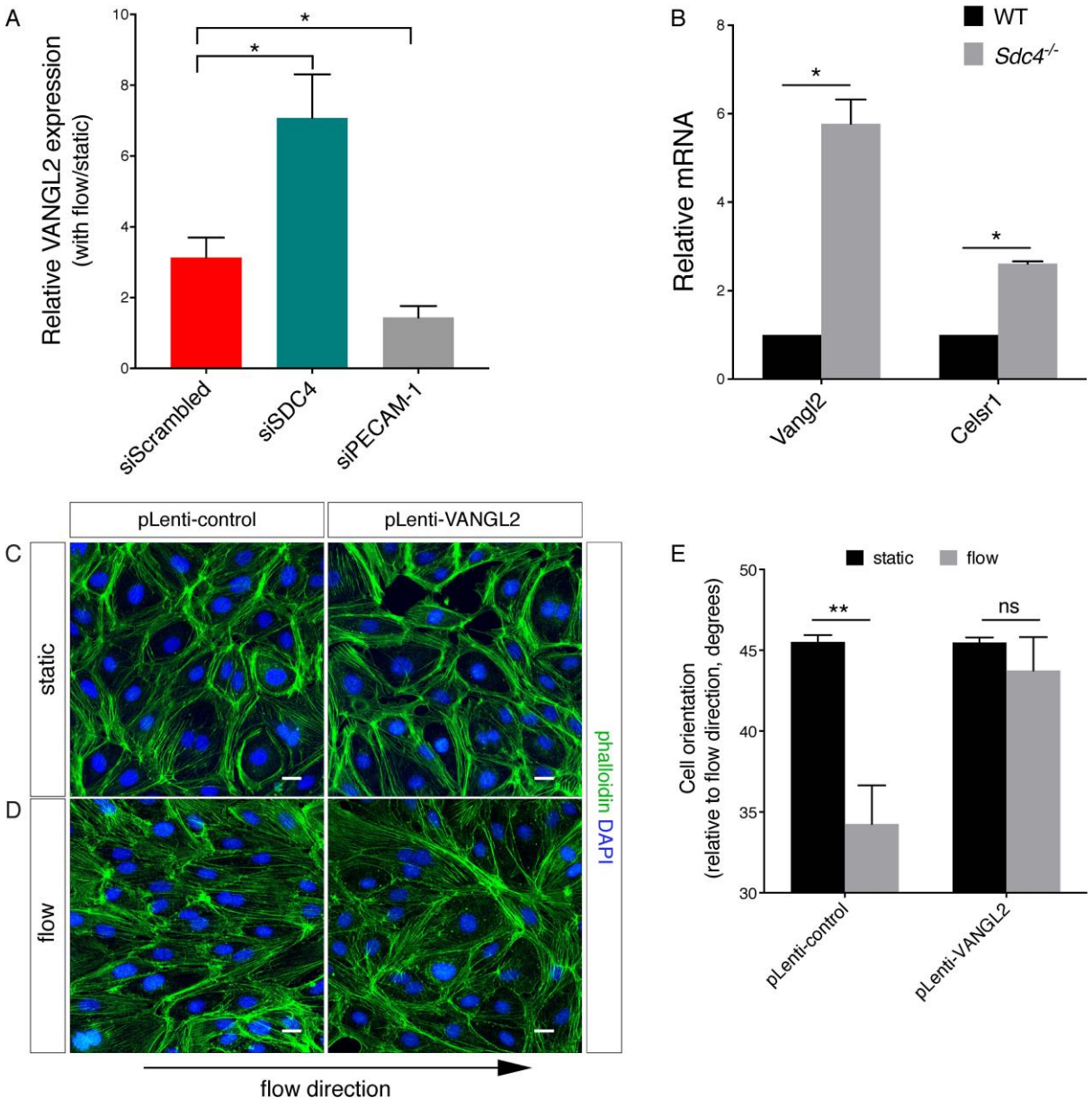

Fig. 6. PCP protein Vangl2 is up-regulated in LECs in *Sdc4*$^{-/-}$ mice. (A) Relative VANGL2 expression in LECs after subjected to laminar flow (8 dynes/cm^2) for 20 hours versus static cells. qRT-PCR analysis. mRNA expression was normalized in relation to the expression of endogenous β-actin. Mann-Whitney test (n = 6). Values represent mean ± SEM. (B) qRT-PCR for Vangl2 and Celsr1 in thoracic ducts of WT and *Sdc4*$^{-/-}$ mice. mRNA expression was normalized in relation to the expression of endogenous 18S rRNA and Cdh5. Mann-Whitney

test (n = 4). Values are mean ± SEM. (C-D) Visualization of the orientation of control LECs (pLenti-control) (C, D, left) and cells overexpressing VANGL2 (pLenti-VANGL2) (C, D, right) by phalloidin (green) and DAPI (blue) labeling. VANGL2 overexpressing LECs do not align to flow direction (D, right). Scale bars: 20um. (E) Quantification of cell orientation of control LECs (pLenti-control) and VANGL2 overexpressing (pLenti-VANGL2) LECs. Cells were either maintained in no flow condition (static) or subjected to laminar flow (8 dynes/cm^2) for 16 hours. One-way ANOVA. ns = non-significant, **: $p<0.01$. n> 2700 cells/condition/experiment. Four independent experiments were performed. Values are mean ± SEM.

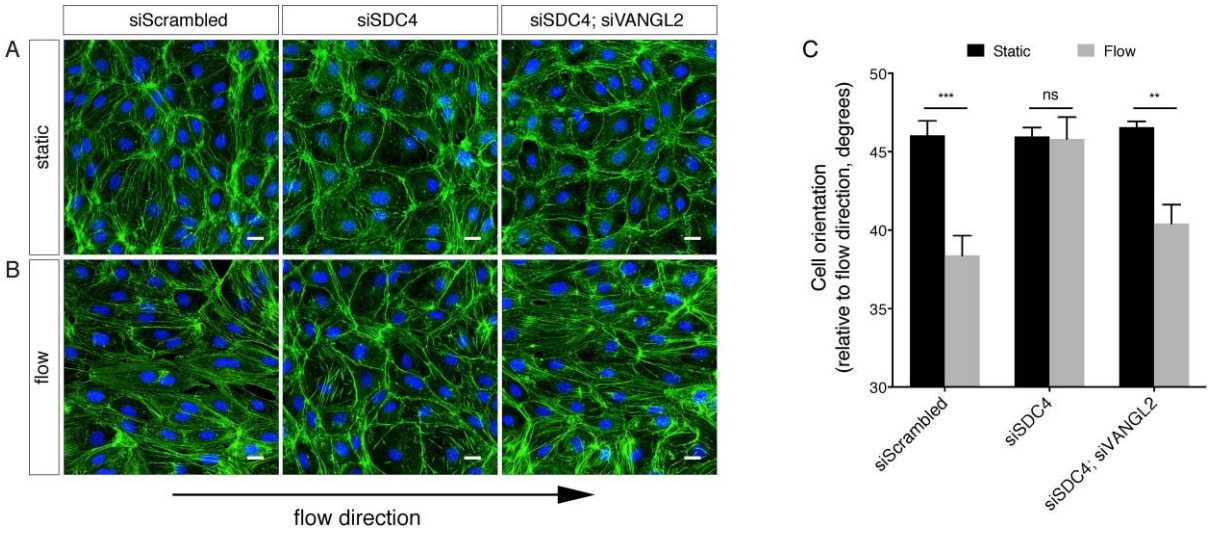

Fig. 7. Syndecan 4 controls flow sensing in LECs through Vangl2.

(A,B) Phalloidin (green) and DAPI (blue) labeling show the arrangement of LECs under static condition (A) and sheared with laminar flow (8 dynes/cm^2) for 16 hours (B). Scale bars: 20um. (C) Quantification of cell orientation of LECs transfected with a scrambled, SDC4 or SDC4 and VANGL2 siRNA. Cells were either cultured at a no flow condition (static) or subjected to laminar flow (8 dynes/cm^2) for 16 hours. 2way ANOVA, ns: non-significant, **: $p<0.01$, ***: $p<0.001$, $n > 1800$ cells/condition/experiment. Four independent experiments were performed. Values are mean ± SEM.

Supplementary figures

Fig. S1.

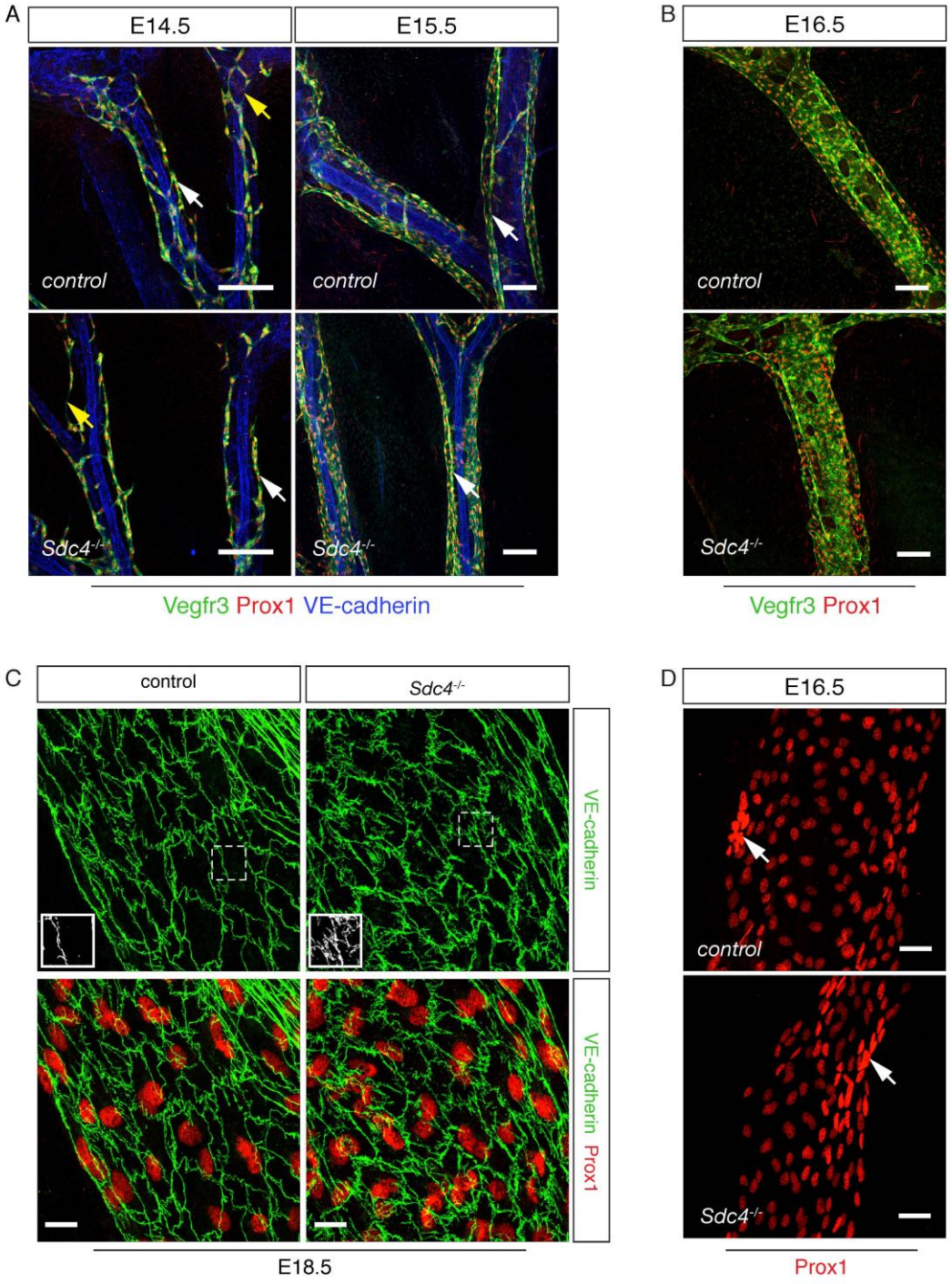

Fig. S1 The development of mesenteric lymphatic vessels in control and *Sdc4*$^{-/-}$ mice. **A,B:** Whole-mount antibody staining of mesenteric lymphatic vessels in control and *Sdc4* null mice at various developmental stages as indicated. Scale bars: 100um. **C:** Whole-mount immunofluorescence staining. LEC cell-cell junctions in *Sdc4* nulls are less linear compared with littermate controls. Inserts are enlarged images of boxed areas. Scale bars: 15um. **D:** Immunostaining for Prox1 showing a cluster of Prox1^{high} lymphatic-valve-forming ECs aligned along lymphatic vessel wall in control (arrow) and *Sdc4*$^{-/-}$ mice (arrow). Scale bars: 30um.

Fig. S2.

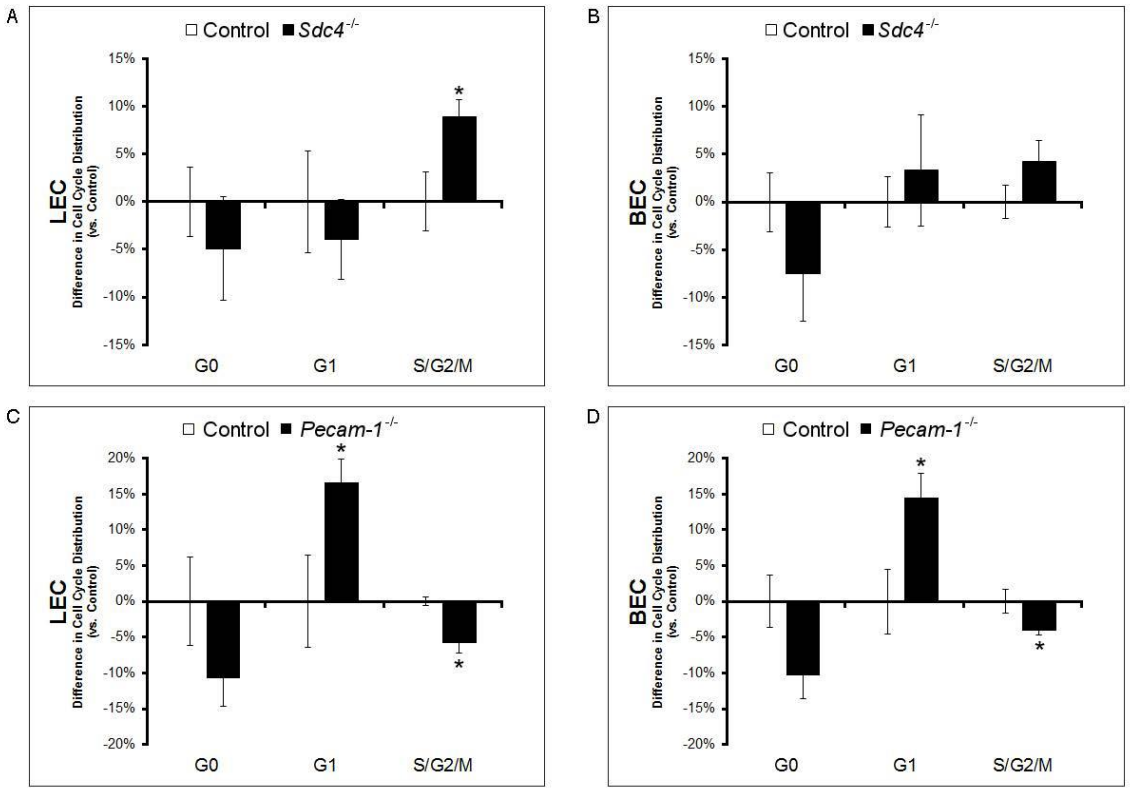

Fig. S2 Cell cycle distribution of LECs and BECs in *Sdc4*$^{-/-}$ and *Pecam-1*$^{-/-}$ mice.

A-D: Analysis of cell cycle distribution of LECs and BECs isolated from mesenteries of E18.5 WT, *Sdc4*$^{-/-}$ (A, B) or *Pecam-1*$^{-/-}$ (C, D) mice using FACS.

Fig. S3.

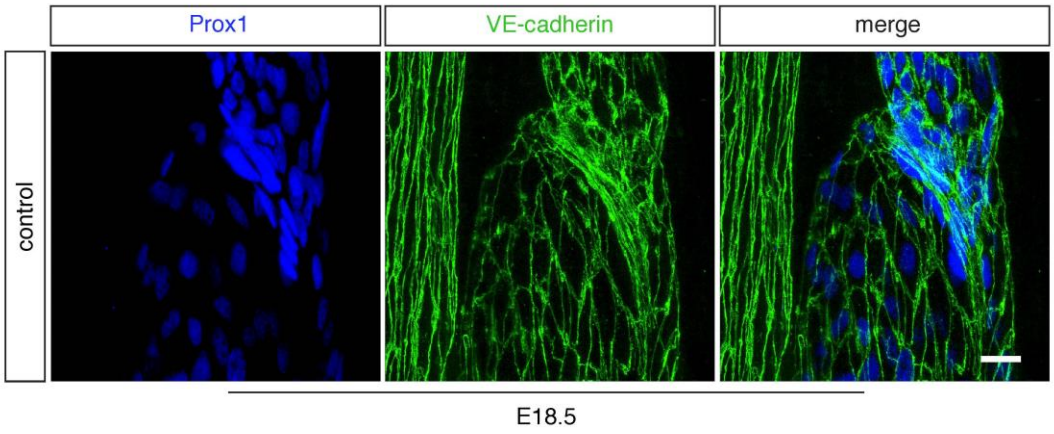

Fig. S3 The morphology and orientation of LECs are correlated with nuclear morphology and orientation. Immunofluorescence labeling for Prox1 (blue) and VE-cadherin (green) showing nuclear morphology and orientation of LECs are highly correlated with cell morphology and orientation in mesenteric lymphatic vessels in control mice. Scale bar: 15um.

Fig. S4.

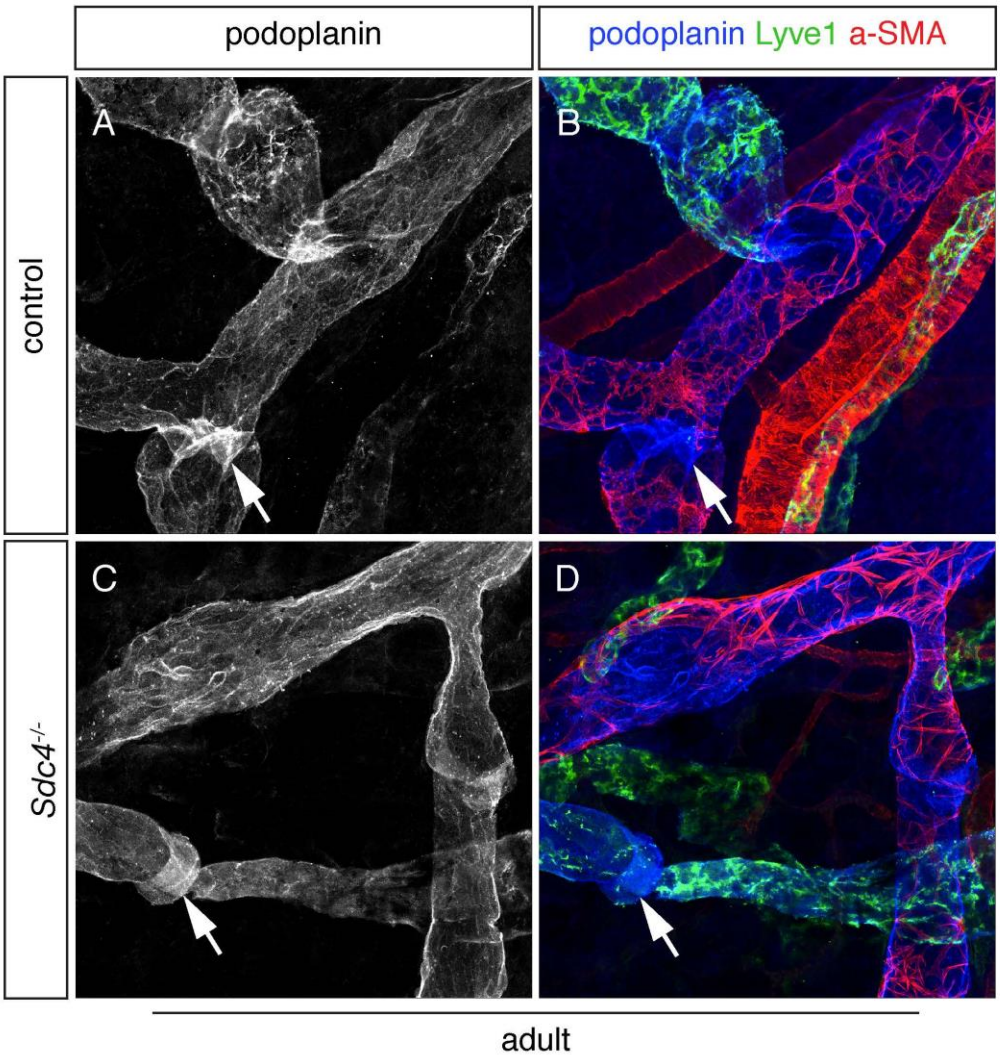

Fig. S4 Abnormal lymphatic valves are observed in *Sdc4* null adult mice. **A-D:** Whole-mount antibody staining of adult mouse ear skin. (A,B) Arrows indicate normal lymphatic valves formed in control mice. (C,D) Arrows indicate abnormal lymphatic valves in *Sdc4* nulls.

Fig. S5.

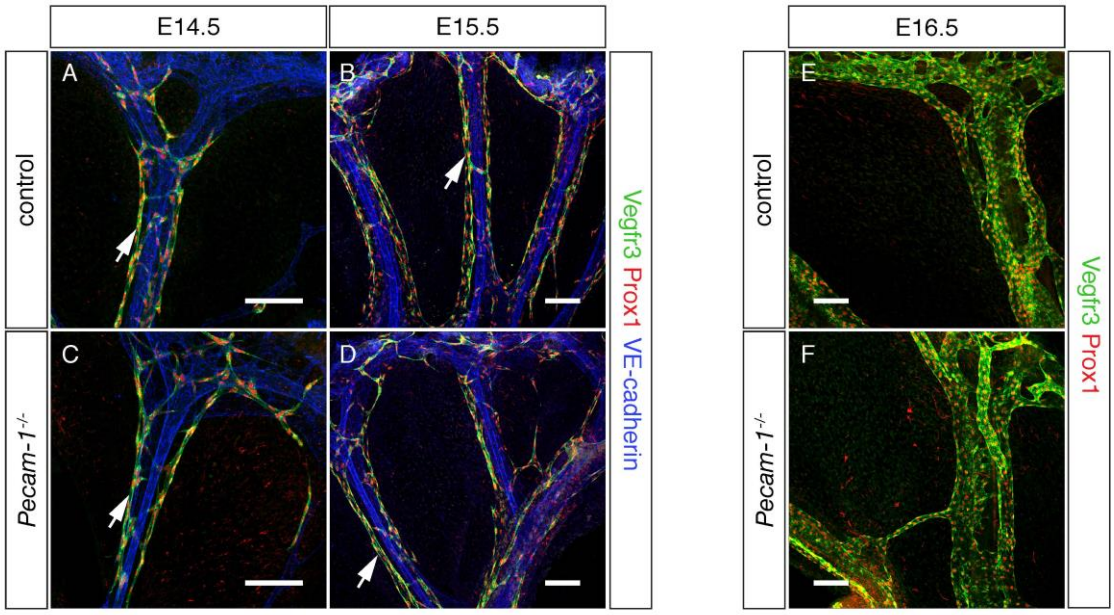

Fig. S5 Lymphatic vessels are developed normally in *Pecam-1*$^{-/-}$ mice from E14.5 to E16.5. **A-F:** Formation of mesenteric lymphatic vessels (Prox1+, Vegfr3+, VE-cadherin+) in *Pecam1*$^{-/-}$ mice (C, D, arrows, and F) is similar as in controls (A, B, arrows and E) from E14.5 to E16.5. Scale bars: 100um.

Fig. S6.

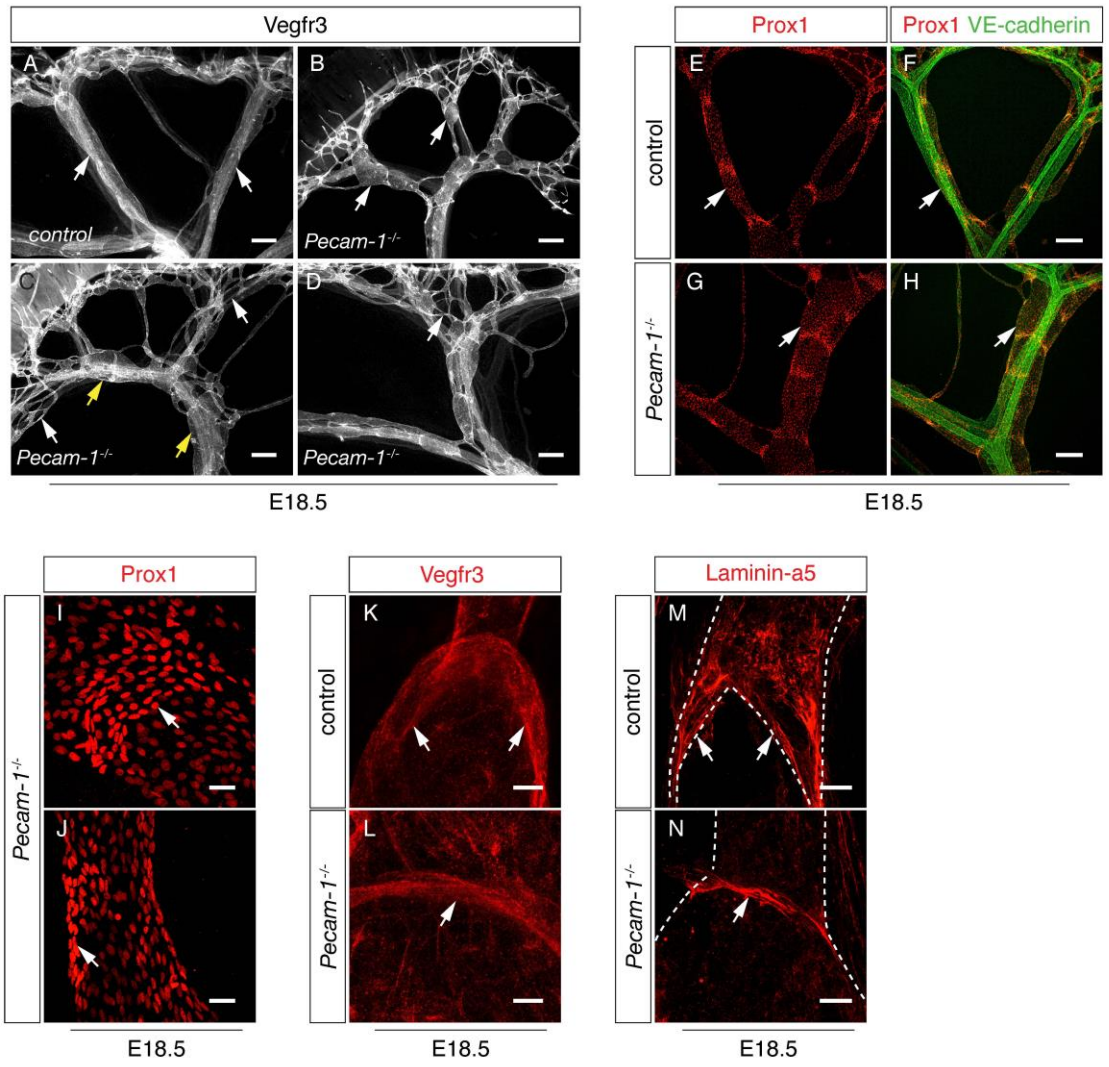

Fig. S6 *Pecam-1* null mice exhibit lymphatic remodeling defects at E18.5. **A-H:** Irregular (B, arrows), enlarged (C, yellow arrows, G, H, arrows) and abnormally branched (C, white arrows, D, arrow) mesenteric lymphatic vessels are developed in *Pecam-1* knockout mice at E18.5 but not in controls (A, E and F, arrows). Scale bars: 200um.

I-J: Antibody staining for Prox1 shows less elongated (I, arrow), loosely organized (I) nuclei of Prox1^{high} lymphatic-valve-forming ECs in *Pecam-1* null mice. Prox1^{high} valve-forming cells remained to the longitudinal axis of lymphatic vessels are observed in *Pecam-1* nulls at E18.5 (J, arrow). Scale bars: 30um. **K-N:** Ring-shape immature lymphatic valves developed in *Pecam-1*$^{-/-}$ animals (L, N, arrows). Leaflets of mature lymphatic valves in control mice (K, M, arrows). Scale bars: K-L, 10um; M-N, 15um.

Fig. S7.

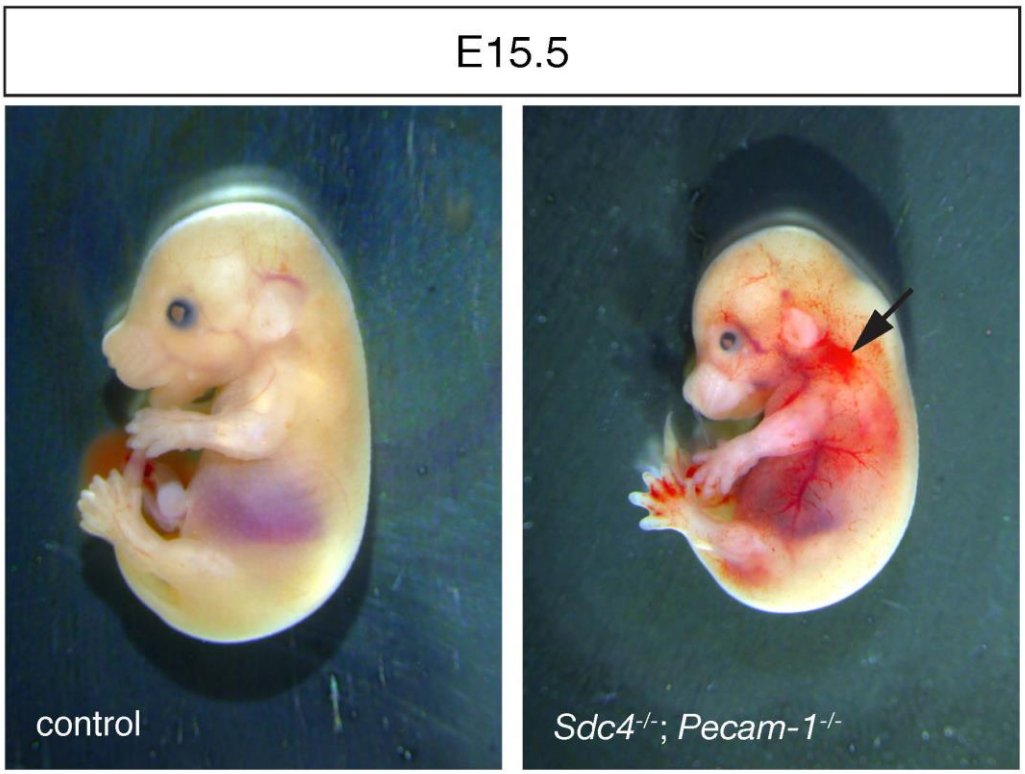

Fig. S7 Blood-filled jugular lymph sac is developed in *Sdc4*$^{-/-}$; *Pecam-1*$^{-/-}$ mouse. Grossly dissected control and *Sdc4*$^{-/-}$; *Pecam-1*$^{-/-}$ mouse embryos at E15.5. Arrow indicates blood-filled jugular lymph sac.

Fig. S8.

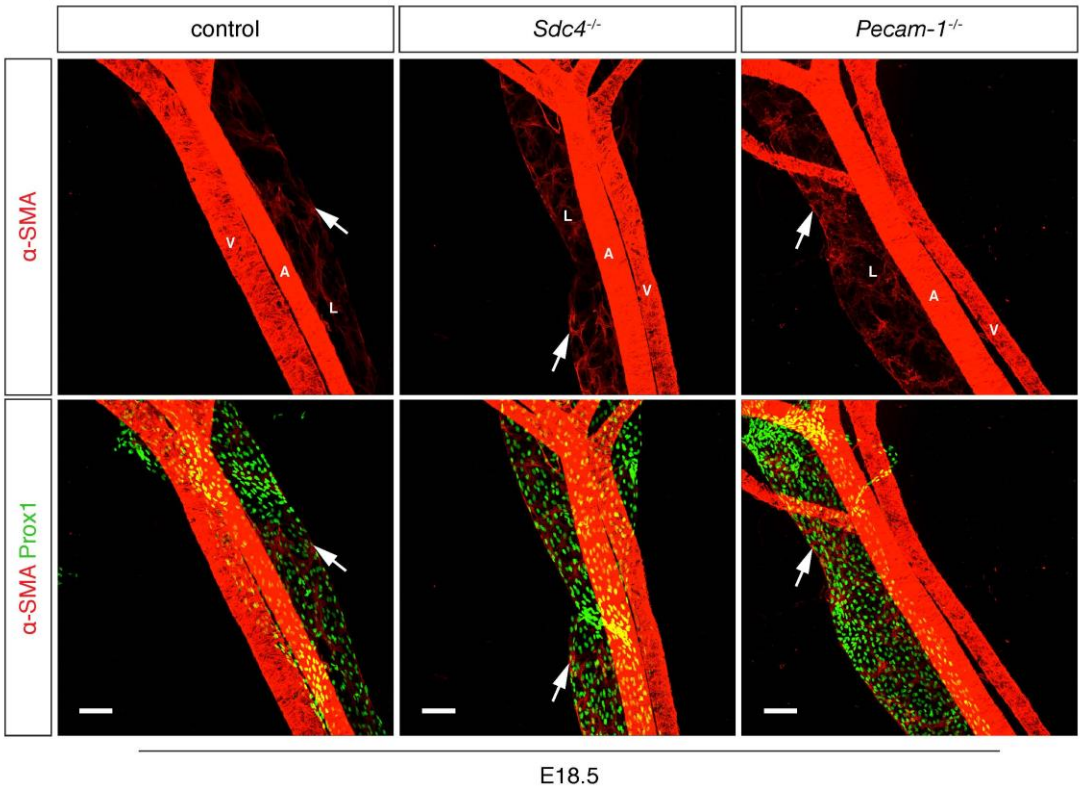

Fig. S8 Increased mural cell coverage in lymphatic vessels in *Sdc4*$^{-/-}$ or *Pecam-1*$^{-/-}$ mice. Mural cell (a-SMA+) recruitment in mesenteric lymphatic vessels in *Sdc4*$^{-/-}$ (arrows) or *Pecam-1*$^{-/-}$ (arrows) mice is increased compared to littermate controls (arrows). A=artery, V=vein, L=lymphatics. Scale bars: 100um.

Fig. S9.

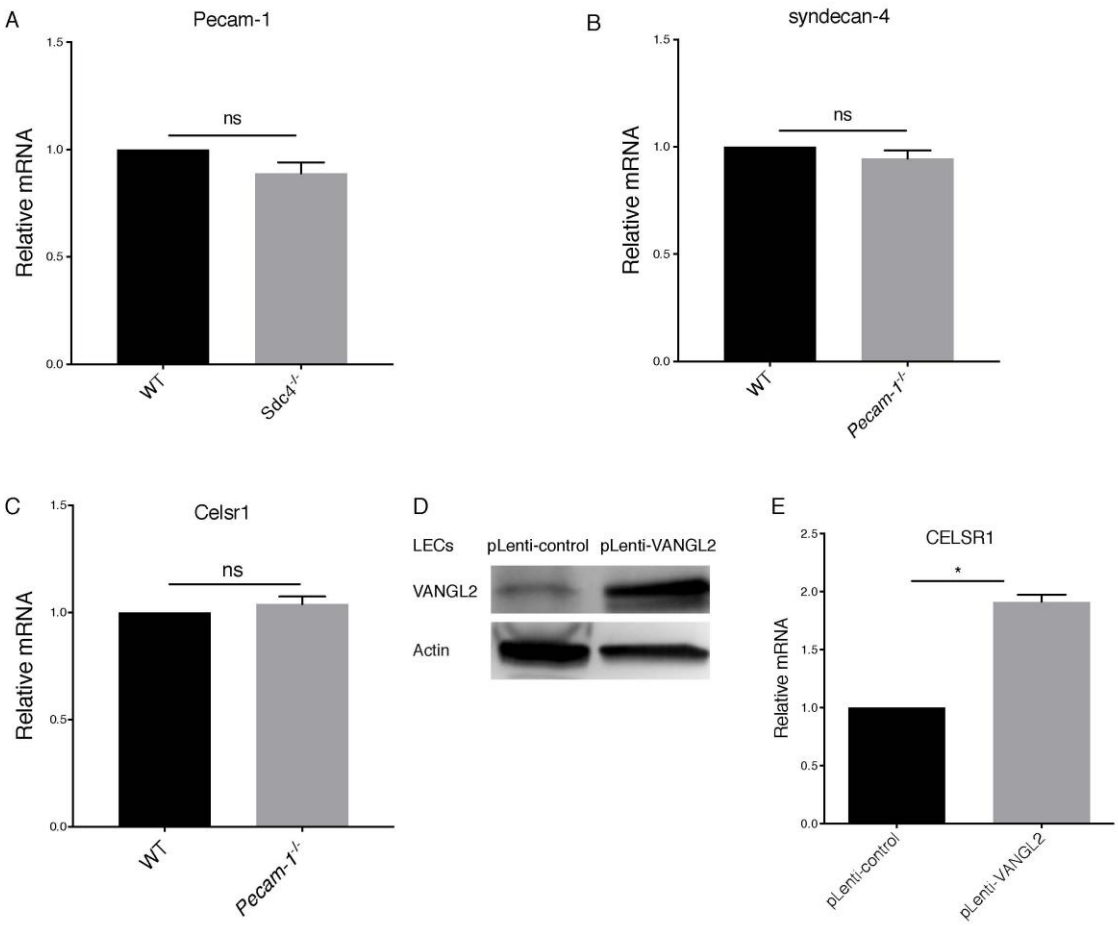

Fig. S9 qRT-PCR and western blotting analysis. **A-C:** qRT-PCR for various gene expression in thoracic duct of WT, *Sdc4*$^{-/-}$ or *Pecam-1*$^{-/-}$ mice. mRNA expression was normalized in relation to the expression of endogenous 18S rRNA. Mann-Whitney test (n = 4 (A, B), n=7 (C)). Values are mean ± SEM. **D:** Western blotting shows VANGL2 overexpression in LECs transduced with a lentivirus expressing VANGL2 (pLenti-VANGL2). **E:** qRT-PCR for CELSR1 expression in control LECs (pLenti-control) or cells overexpressing VANGL2 (pLenti-VANGL2). mRNA expression was normalized in

relation to the expression of endogenous β-actin. Mann-Whitney test (n = 4). Data represents mean ± SEM.

Fig. S10.

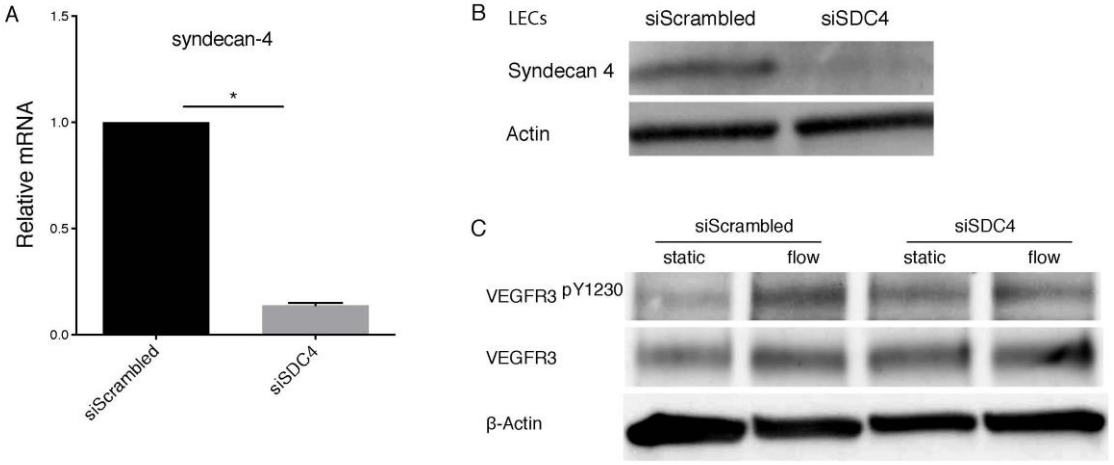

Fig. S10 Flow-induced activation of VEGFR3 signaling is reduced in *SDC4* KD LECs compared with controls. **A, B:** qRT-PCR (A) and western blotting (B) show reduced syndecan-4 expression in LECs transfected with siRNA against SDC4. mRNA expression was normalized in relation to the expression of endogenous β-actin. Mann-Whitney test (n = 4). Data are mean ± SEM. **C:** Western blotting shows flow-induced activation of VEGFR3 signaling.

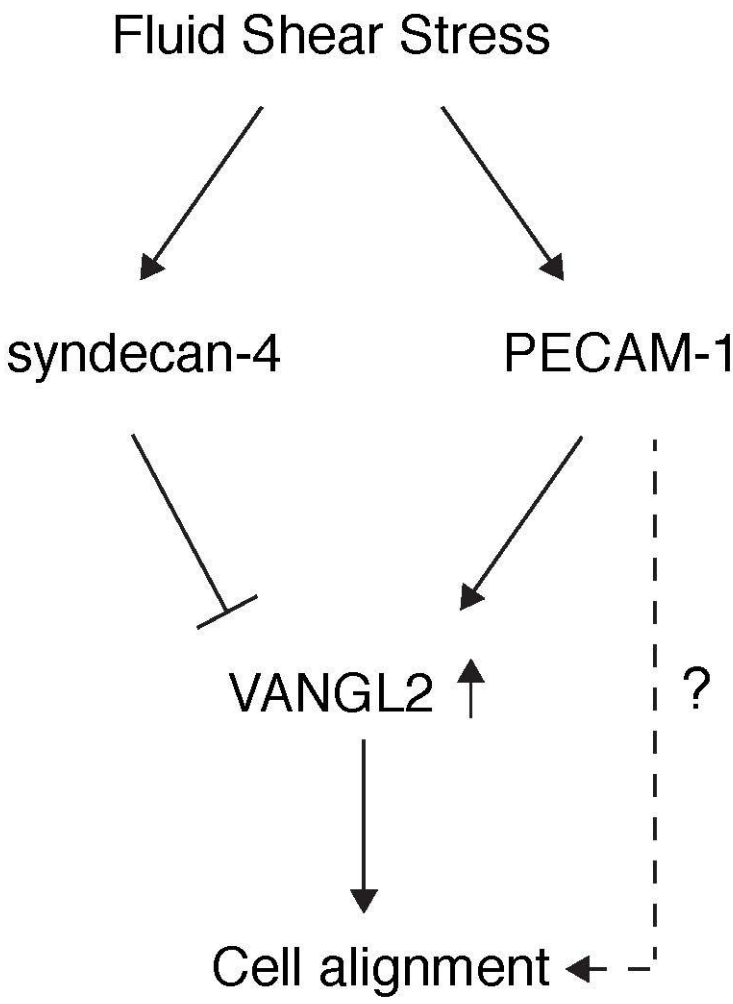

Fig. S11 A scheme illustrating syndecan-4 and PECAM-1 controlled flow signaling in LECs. Fluid shear stress transduced by the mechanosensory complex consisting PECAM-1/VE-cadherin/VEGFR2/3 up-regulates PCP protein VANGL2 in LEC. Syndecan-4-mediated flow signals ensures flow-induced VANGL2 expression within a certain range, which is critical for LECs to align to flow. In the absence of syndecan-4, flow-induced

VANGL2 expression are too high, cells fail to align. The mechanism of PECAM-1 controlled flow signaling in LECs remains unknown.